nature methods

RESOURCE

https://doi.org/10.1038/s41592-018-0189-6

A mutant-cell library for systematic analysis of heparan sulfate structure–function relationships

Hong Qiu[1,2], Songshan Shi[1,3], Jingwen Yue[1,2], Meng Xin[1,2], Alison V. Nairn[1], Lei Lin[4], Xinyue Liu[4], Guoyun Li[5], Stephanie A. Archer-Hartmann[1], Mitche Dela Rosa[1], Melina Galizzi[1], Shunchun Wang[1,3], Fuming Zhang[4], Parastoo Azadi[1], Toin H. van Kuppevelt[6], Wellington V. Cardoso[7], Koji Kimata[8], Xingbin Ai[9], Kelley W. Moremen[1,2], Jeffrey D. Esko[10], Robert J. Linhardt[4] and Lianchun Wang[1,2*]

Heparan sulfate (HS) is a complex linear polysaccharide that modulates a wide range of biological functions. Elucidating the structure–function relationship of HS has been challenging. Here we report the generation of an HS-mutant mouse lung endothelial cell library by systematic deletion of HS genes expressed in the cell. We used this library to (1) determine that the strictly defined fine structure of HS, not its overall degree of sulfation, is more important for FGF2–FGFR1 signaling; (2) define the epitope features of commonly used anti-HS phage display antibodies; and (3) delineate the fine inter-regulation networks by which HS genes modify HS and chain length in mammalian cells at a cell-type-specific level. Our mutant-cell library will allow robust and systematic interrogation of the roles and related structures of HS in a cellular context.

HS is a linear polysaccharide with a complex structure. HS varies considerably in size, position, and degree of sulfation, as well as in epimerization of uronic acid in different cells, tissues, and developmental stages. Such structural complexity and spatial and temporal expression patterns form the basis of the multifaceted functions of HS.

Biochemical studies with small-sized HS oligosaccharides and chemically modified heparins, a highly sulfated form of HS, have shown that HS interacts with protein ligands through its unique binding sites, which consist of relatively small tracts of variable modifications, including N-sulfation (NS), 6-O-sulfation (6S), and 3-O-sulfation (3S) of glucosamine residues; 2-O-sulfation (2S) of uronic acid; and epimerization of glucuronic acid to iduronic acid (IdoA), in specific arrangements[1–3] (Fig. 1a). Extension of the biochemical findings to a cellular level is essential for a better understanding of the structure–function relationships and unique biological and pathological roles of HS. However, this has been challenging owing to the length of native HS and its propensity to interact simultaneously with a ligand and the ligand's receptor or to harbor multiple copies of binding sites for a ligand[1,4,5]. In addition, the relative importance of fine structures versus overall sulfation of HS in interaction with a protein ligand remains a fundamental question in HS biology[6–9]. Furthermore, anti-HS phage display antibodies have been widely used to probe specific HS structures in situ, but their native HS epitope structures remain unclear. Better characterization of the HS epitope features might yield valuable new information for future antibody-based studies.

Here we report the development of an HS-mutant mouse lung endothelial cell (MLEC) library that enabled us to address some of the aforementioned fundamental HS biology issues, and which represents a novel test platform for systematic interrogation of the roles and related structures of HS in a cellular context.

Results

Generation of an HS-mutant MLEC library. To generate a comprehensive HS-mutant MLEC library that targeted all the HS-expressing genes in the cells, we first carried out qRT-PCR analysis to profile HS-gene expression in primary MLECs. In mammals, there are as many as 20 HS-specific genes that function to biosynthesize HS, as well as two genes involved in postbiosynthetic remodeling. Among these genes, 12 are expressed in mice: the chain polymerization genes exostosin 1 (*Ext1*) and *Ext2*; the modification genes N-deacetylase/N-sulfotransferase 1 (*Ndst1*) and *Ndst2*; glucuronyl C5-epimerase (*Glce*); HS 2-O-sulfotransferase 1 (*Hs2st1*); HS 6-O-sulfotransferase 1 (*Hs6st1*) and *Hs6st2*; HS (glucosamine) 3-O-sulfotransferase 1 (*Hs3st1*) and *Hs3st4*; and the remodeling genes HS 6-O-endosulfatase 1 (*Sulf1*) and *Sulf2* (Fig. 1b).

We targeted all these HS-expressing genes. By means of cell immortalization and cloning (Supplementary Fig. 1), we derived MLEC lines directly from 8–10-week-old $Ext1^{f/f}$, $Ndst1^{f/f}$, $Ndst1^{f/f}$;$Ndst2^{-/-}$, $Hs2st1^{f/f}$, $Hs6st1^{f/f}$, $Hs6st1^{f/f}$;$Hs6st2^{-/-}$, and $Sulf1^{f/f}$;$Sulf2^{f/f}$ mice. We further subjected these cell lines to transient Cre recombinase expression to derive the corresponding mutant $Ext1^{-/-}$, $Ndst1^{-/-}$, $Ndst1^{-/-}$;$Ndst2^{-/-}$, $Hs2st1^{-/-}$, $Hs6st1^{-/-}$, $Hs6st1^{-/-}$;$Hs6st2^{-/-}$ and

[1]Complex Carbohydrate Research Center, University of Georgia, Athens, GA, USA. [2]Department of Biochemistry and Molecular Biology, University of Georgia, Athens, GA, USA. [3]Institute of Materia Medica, Shanghai University of Traditional Chinese Medicine, Shanghai, China. [4]Departments of Chemistry and Chemical Biology, Chemical and Biological Engineering, and Biomedical Engineering, Center for Biotechnology and Interdisciplinary Studies, Rensselaer Polytechnic Institute, Troy, NY, USA. [5]Key Laboratory of Marine Drugs, Ministry of Education, School of Medicine and Pharmacy, Shandong Provincial Key Laboratory of Glycoscience and Glycotechnology, Ocean University of China, Qingdao, China. [6]Department of Biochemistry, Radboud Institute for Molecular Life Sciences, Radboud University Medical Centre, Nijmegen, the Netherlands. [7]Division of Pulmonary and Critical Care Medicine, Department of Medicine, Columbia University Medical Center, New York, NY, USA. [8]Multidisciplinary Pain Center, Aichi Medical University, Nagakute, Japan. [9]Division of Pulmonary and Critical Care Medicine, Brigham and Women's Hospital, Harvard Medical School, Boston, MA, USA. [10]Glycobiology Research and Training Center, Department of Cellular and Molecular Medicine, University of California San Diego, La Jolla, CA, USA.
*e-mail: Lwang@ccrc.uga.edu

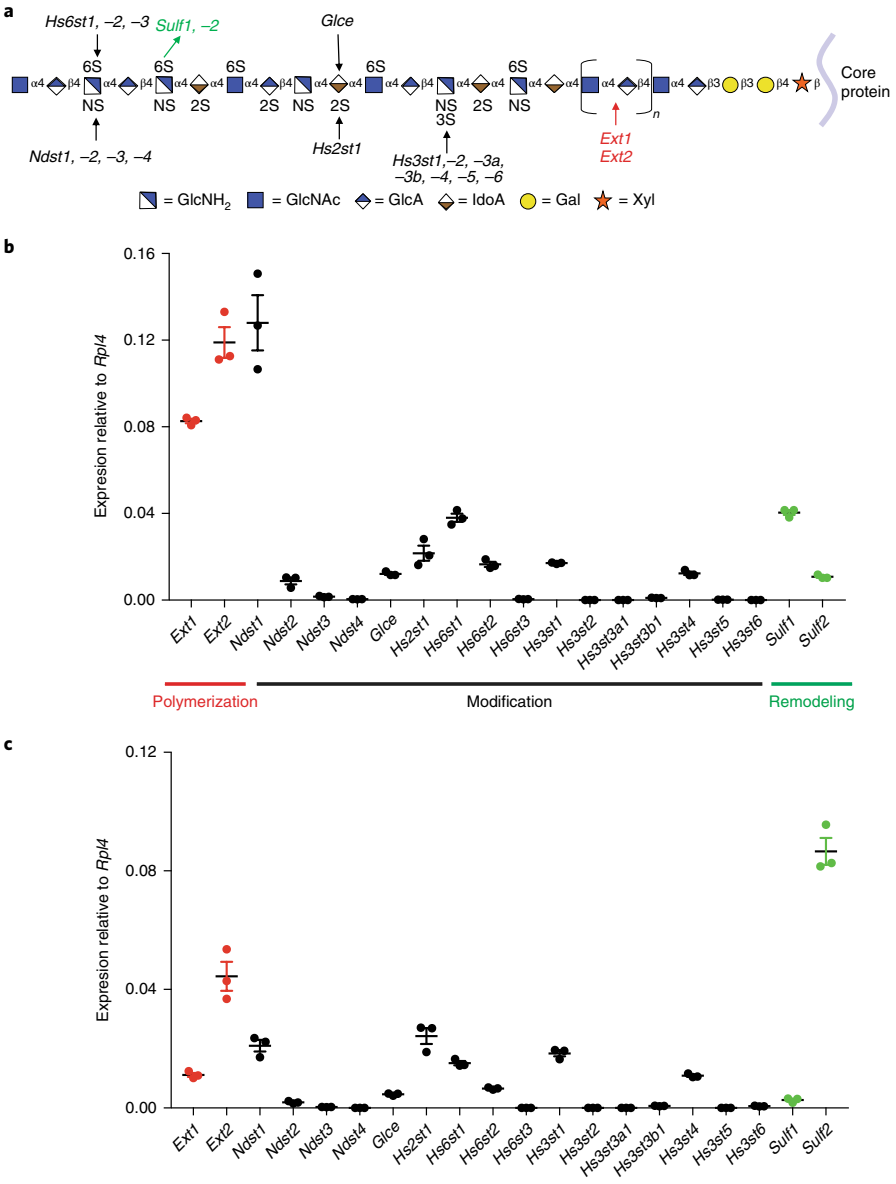

Fig. 1 | Expression of HS biosynthetic and remodeling genes in MLECs. a, HS structure and the biosynthetic/remodeling genes that affect various aspects of that structure. Each sugar residue is depicted by a symbol according to the key. $GlcNH_2$, glucosamine; GlcNAc, N-acetylglucosamine; GlcA, glucuronic acid; IdoA, iduronic acid; Gal, galactose; Xyl, xylose. **b**,**c**, Expression patterns of HS polymerization, modification, and remodeling genes in primary (**b**) and immortalized (**c**) MLECs as determined by qRT-PCR analysis. The data are representative of 3 independent experiments and are presented as mean ± s.d.

Sulf1$^{-/-}$;*Sulf2*$^{-/-}$ cell lines. All seven directly derived MLEC lines expressed endothelial cell markers CD31 and VEGFR2, which confirmed their endothelial cell identity (Supplementary Fig. 2). The HS-gene expression patterns in the *Ext1*$^{f/f}$, *Ndst1*$^{f/f}$, *Hs2st1*$^{f/f}$, *Hs6st1*$^{f/f}$, and *Sulf1*$^{f/f}$;*Sulf2*$^{f/f}$ MLEC lines were similar to those in primary MLECs (Fig. 1b,c and Supplementary Fig. 3), which indicated that the derived mutant cell lines might closely reflect HS structure alterations in vivo after targeted gene deletion. We did not collect the mice deficient for *Glce*, *Hs3st1*, or *Hs3st4* because of their embryonic lethality or unavailability. Instead, we transiently cotransfected the *Ndst1*$^{f/f}$ MLEC line with Cas9 and guide RNA (gRNA) specific for *Glce*, *Hs3st1*, or *Hs3st4* (Supplementary Figs. 1 and 4). After screening for induced genomic insertion/deletion (indel) mutations and confirming the indels by sequencing the gRNA-targeted regions, we obtained *Glce*$^{-/-}$, *Hs3st1*$^{-/-}$, *Hs3st4*$^{-/-}$, and *Hs3st1*$^{-/-}$;*Hs3st4*$^{-/-}$ MLEC lines (Supplementary Fig. 4). By deleting HS-expressing genes individually or in combination, we developed an HS-mutant MLEC library containing a total of 18 cell lines and harboring alterations of all HS modification types (Table 1).

Characterization of HS structure expression in mutant MLECs. We next characterized the generated mutant cells to understand HS alteration after HS-gene deletion. As we reported previously[10–12], *Ext1* deletion decreases HS expression, as reflected by decreased staining for anti-HS (clone 10E4) (Fig. 2a). The other HS-mutant cell lines all expressed HS. We analyzed them for HS disaccharide

Table 1 | HS disaccharide composition and molecular weight in derived MLEC lines

Cell lines	Gene-editing approach	NAc	NS	2S	6S	Total sulfate	Molecular weight (kDa)
Ext1$^{f/f}$	Cre-*loxP*	33.47 ± 0.64	56.28 ± 0.35	21.64 ± 0.71	14.63 ± 0.38	92.55	14
Ext1$^{-/-}$		n.a.	n.a.	n.a.	n.a.	n.a.	n.a.
Ndst1$^{f/f}$	Cre-*loxP*	32.61 ± 3.38	58.69 ± 3.28	17.29 ± 1.95	16.35 ± 1.67	94.07	15
Ndst1$^{-/-}$		70.71 ± 2.51	22.75 ± 2.59	5.18 ± 1.04	10.08 ± 1.02	38.02	15
WTa*	Direct derivation	33.54 ± 2.54	56.77 ± 2.04	17.72 ± 2.91	17.02 ± 2.47	92.66	14.4
Ndst1$^{f/f}$;*Ndst2*$^{-/-}$	and Cre-*loxP*	48.85 ± 8.48	39.14 ± 7.38	10.30 ± 6.91	16.36 ± 1.12	65.80	13
Ndst1$^{-/-}$;*Ndst2*$^{-/-}$		91.50 ± 0.76	2.93 ± 0.56	2.53 ± 0.90	3.47 ± 1.13	10.58	17
WT (*Ndst1*$^{f/f}$)#	CRISPR–Cas9	32.61 ± 3.38	58.69 ± 3.28	17.29 ± 1.95	16.35 ± 1.67	94.07	15
Glce$^{-/-}$		23.12 ± 0.27	72.50 ± 0.25	6.84 ± 0.26	33.53 ± 0.58	107.73	14
Hs2st1$^{f/f}$	Cre-*loxP*	31.99 ± 2.59	59.06 ± 3.10	18.67 ± 2.82	17.55 ± 2.82	95.28	14
Hs2st1$^{-/-}$		21.92 ± 3.77	72.23 ± 2.71	0	29.96 ± 5.23	102.20	17
Hs6st1$^{f/f}$	Cre-*loxP*	37.92 ± 5.36	54.41 ± 5.26	17.58 ± 2.10	15.03 ± 1.36	87.02	12
Hs6st1$^{-/-}$		36.06 ± 5.20	58.05 ± 5.76	19.16 ± 2.17	8.40 ± 0.30	85.61	16
WTa*	Direct derivation	33.54 ± 2.54	56.77 ± 2.04	17.72 ± 2.91	17.02 ± 2.47	92.66	14.4
Hs6st1$^{f/f}$;*Hs6st2*$^{-/-}$	and Cre-*loxP*	37.03 ± 0.48	54.45 ± 0.32	13.29 ± 0.65	17.78 ± 0.25	85.52	12
Hs6st1$^{-/-}$;*Hs6st2*$^{-/-}$		31.80 ± 1.54	66.30 ± 1.12	26.41 ± 1.82	0.08 ± 0.14	92.79	16
WT (*Ndst1*$^{f/f}$)#	CRISPR–Cas9	32.61 ± 3.38	58.69 ± 3.28	17.29 ± 1.95	16.35 ± 1.67	94.07	15
Hs3st1$^{-/-}$		34.52 ± 3.86	54.98 ± 3.41	20.10 ± 1.57	16.95 ± 0.58	94.24	11
Hs3st4$^{-/-}$		37.30 ± 3.11	55.65 ± 2.51	18.03 ± 1.47	10.73 ± 1.28	84.15	16
Hs3st1$^{-/-}$;*Hs3st4*$^{-/-}$		39.62 ± 3.16	51.25 ± 4.06	18.88 ± 2.90	11.26 ± 2.45	82.48	15
Sulf1$^{f/f}$;*Sulf2*$^{f/f}$	Cre-*loxP*	31.71 ± 0.55	55.38 ± 0.51	18.59 ± 0.34	20.42 ± 0.36	94.39	15
Sulf1$^{-/-}$;*Sulf2*$^{-/-}$		34.96 ± 0.18	50.51 ± 1.32	14.18 ± 1.50	27.21 ± 0.96	91.91	18

Eighteen MLEC lines were generated, including 5 'wild-type' (WT; in which the HS-specific genes were conditionally targeted) and 13 HS-mutant cell lines. The HS-mutant cell lines were derived from conditionally targeted HS gene alleles by Cre recombinase treatment (Cre-*loxP* gene targeting) or conventional HS mutant alleles, or by direct gene targeting with gRNA (CRISPR–Cas9 approach). WTa, average of the five immortalized WT MLEC lines (*Ext1*$^{f/f}$, *Ndst1*$^{f/f}$, *Hs2st1*$^{f/f}$, *Hs6st1*$^{f/f}$, and *Sulf1*$^{f/f}$;*Sulf2*$^{f/f}$). NAc, N-acetyl group; NS, N-sulfate; 2S, 2-O-sulfate; 6S, 6-O-sulfate. The data were summarized from 3 independent experiments and are presented as mean ± s.d., except for the molecular weight, which was measured only one time per cell line. *Data were pooled from the five WT MLEC lines as a control for the mutant cell lines that were directly derived from the corresponding conventional HS-mutant mice. #The parental *Ndst1*$^{f/f}$ MLEC line was used as the WT control for CRISPR–Cas9-derived HS-mutant cell lines.

composition by digesting isolated HS with heparinases I–III and separating the resulting disaccharide with an anion-exchange column in an HPLC system (Supplementary Data). For the Cre-*loxP*-derived HS mutants, we used the corresponding floxed cell lines as controls (the floxed control cell lines are referred to as wild-type controls here for convenience). For the *Ndst1*$^{f/f}$;*Ndst2*$^{-/-}$, *Ndst1*$^{-/-}$;*Ndst2*$^{-/-}$, *Hs6st1*$^{f/f}$;*Hs6st2*$^{-/-}$ and *Hs6st1*$^{-/-}$;*Hs6st2*$^{-/-}$ lines that were originally derived from conventional gene-knockout mice, we used data pooled from the five 'wild-type' MLEC lines (*Ext1*$^{f/f}$, *Ndst1*$^{f/f}$, *Hs2st1*$^{f/f}$, *Hs6st1*$^{f/f}$ and *Sulf1*$^{f/f}$;*Sulf2*$^{f/f}$) as the control (WTa, where "a" indicates the average). We generated the *Glce*$^{-/-}$, *Hs3st1*$^{-/-}$, *Hs3st4*$^{-/-}$ and *Hs3st1*$^{-/-}$;*Hs3st4*$^{-/-}$ lines via CRISPR–Cas9 technology, and used the parent *Ndst1*$^{f/f}$ line as the wild-type control.

We first examined samples with alterations in *Ndst*-family genes. HS in *Ndst1*$^{-/-}$ cells showed a 40–60% reduction in NS, 2S, and 6S compared with levels in the control (NS 58.7%, 2S 17.3%, and 6S 16.4% in *Ndst1*$^{f/f}$, versus NS 22.7%, 2S 5.2%, and 6S 10.0% in *Ndst1*$^{-/-}$) (Fig. 2b, Table 1). HS in *Ndst2*$^{-/-}$ cells showed a less pronounced reduction in these modifications, and HS in *Ndst1*$^{-/-}$;*Ndst2*$^{-/-}$ cells showed decreased sulfation modification (NS 56.8%, 2S 17.7%, and 6S 17.0% in WTa; NS 39.1%, 2S 10.3%, and 6S 16.4% in *Ndst1*$^{f/f}$;*Ndst2*$^{-/-}$; NS 2.9%, 2S 2.5%, and 6S 3.5% in *Ndst1*$^{-/-}$;*Ndst2*$^{-/-}$) (Fig. 2c, Table 1). The overall sulfation was reduced by 59.6% for *Ndst1*$^{-/-}$ HS, 29.0% for *Ndst2*$^{-/-}$ HS, and 88.6% for *Ndst1*$^{-/-}$;*Ndst2*$^{-/-}$ HS compared with that in the control. These *Ndst* mutants could be used to determine the contribution of both NS and overall sulfation to ligand binding and downstream signaling activation in cells. However, caution would need to be taken, as *Ndst*-deficient HS has reduced levels of 2S and 6S.

Glce and *Hs2st1* are the only members of their gene family that are expressed in mice. *Glce*$^{-/-}$ HS showed reduced 2S and increased NS and 6S (NS 58.7%, 2S 17.3%, and 6S 16.4% for *Ndst1*$^{f/f}$ versus NS 72.5%, 2S 6.8%, and 6S 33.5% for *Glce*$^{-/-}$) (Fig. 2d, Table 1). *Hs2st1*$^{-/-}$ HS showed alterations in disaccharide composition similar to those of *Glce*$^{-/-}$ HS, except with a complete lack of 2S (NS 59.1%, 2S 18.7%, and 6S 17.6% for *Hs2st1*$^{f/f}$ versus NS 72.2%, 2S 0%, and 6S 30.0% for *Hs2st1*$^{-/-}$) (Fig. 2e, Table 1). *Glce*$^{-/-}$ and *Hs2st1*$^{-/-}$ HS showed increased overall sulfation compared with levels in controls (14.5% and 7.3%, respectively). The *Glce*$^{-/-}$ and *Hs2st1*$^{-/-}$ cells could be applied to specifically determine the necessity of IdoA and 2S versus that of the overall sulfation level for ligand binding and downstream signaling, respectively.

The 6S alteration is codetermined by *Hs6st* and *Sulf* genes. *Hs6st1*$^{-/-}$ HS showed reduced 6S compared with levels in controls (NS 54.4%, 2S 17.6%, and 6S 15.0% for *Hs6st1*$^{f/f}$ versus NS 58.1%, 2S 19.2%, and 6S 8.4% for *Hs6st1*$^{-/-}$) (Fig. 2f, Table 1). *Hs6st2*$^{-/-}$ HS had a normal disaccharide composition, whereas *Hs6st1*$^{-/-}$;*Hs6st2*$^{-/-}$ HS completely lacked 6S and showed increases in NS and 2S (NS 56.8%, 2S 17.7%, and 6S 17.0% for WTa; NS 54.5%, 2S 13.3%, and 6S 17.8% for *Hs6st1*$^{f/f}$;*Hs6st2*$^{-/-}$; NS 66.3%, 2S 26.4%, and 6S 0.08% for *Hs6st1*$^{-/-}$;*Hs6st2*$^{-/-}$) (Fig. 2g, Table 1). *Sulf1*$^{-/-}$;*Sulf2*$^{-/-}$ HS showed an increase in 6S with reductions in NS and 2S—an effect opposite that observed in *Hs6st1*$^{-/-}$;*Hs6st2*$^{-/-}$ cells (NS 55.4%, 2S 18.6%, and 6S 20.4% for *Sulf1*$^{f/f}$;*Sulf2*$^{f/f}$ versus NS 50.5%, 2S 14.2%, and 6S 27.2% for *Sulf1*$^{-/-}$;*Sulf2*$^{-/-}$) (Fig. 2h, Table 1). HS in the *Hs6st1*$^{-/-}$, *Hs6st1*$^{f/f}$;*Hs6st2*$^{-/-}$, *Hs6st1*$^{-/-}$;*Hs6st2*$^{-/-}$, and *Sulf1*$^{-/-}$;*Sulf2*$^{-/-}$ lines had a normal overall sulfation level. Cells with knockout of *Hs6st* and *Sulf* genes could thus be used to specifically determine the necessity of 6S, or of higher 6S levels relative to the overall sulfation, for ligand binding and downstream signaling.

In the *Hs3st*-gene mutants, *Hs3st1*$^{-/-}$ HS had a normal HS disaccharide composition, whereas *Hs3st4*$^{-/-}$ and *Hs3st1*$^{-/-}$;*Hs3st4*$^{-/-}$HS

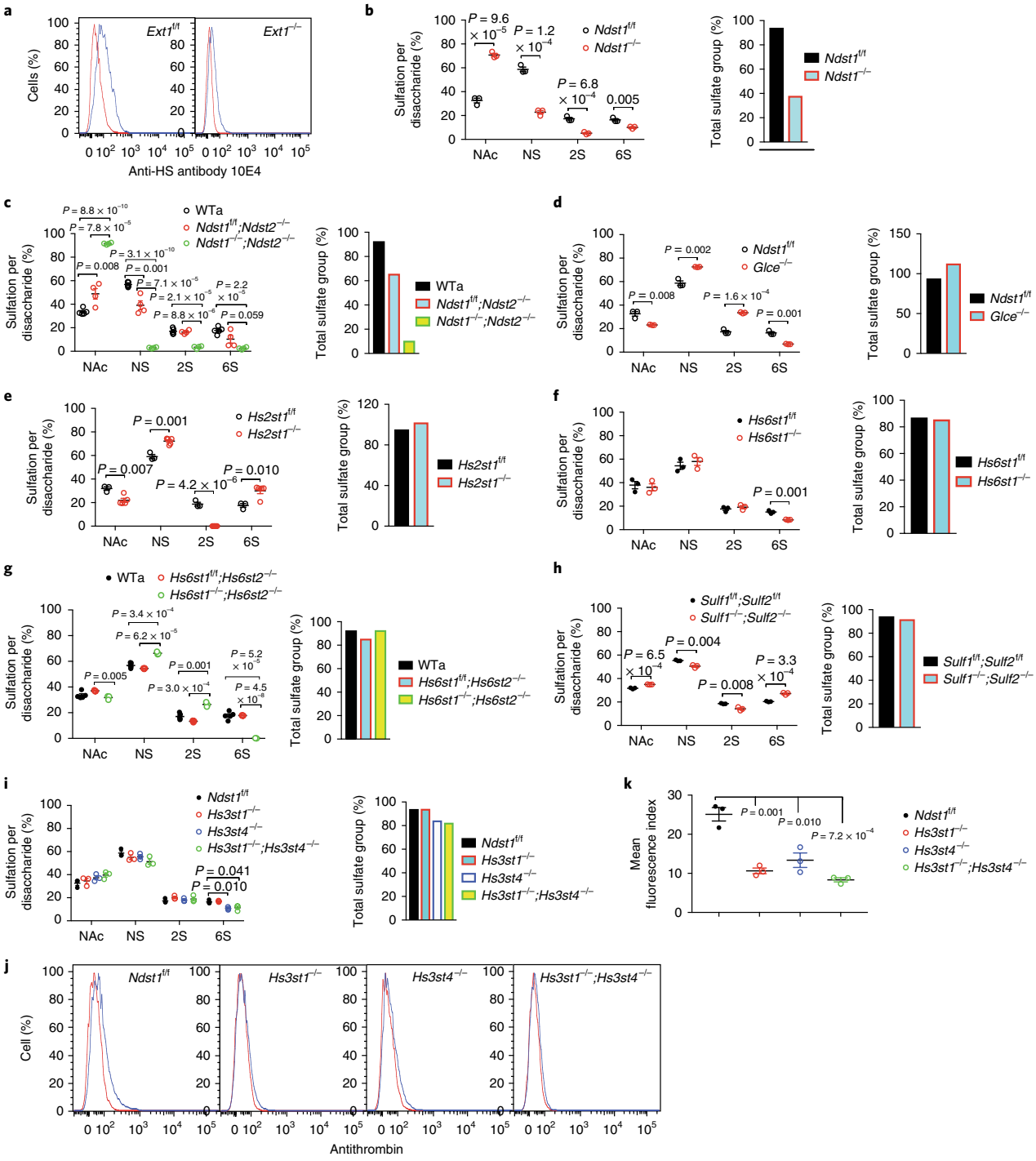

Fig. 2 | HS expression in the generated mutant MLEC lines. a, Cell-surface binding of anti-HS 10E4 as assessed by flow cytometry. **b**–**i**, HS disaccharide composition analysis. HS isolated from mutant MLECs and their corresponding controls was digested with heparinases I–III, and the resulting disaccharides were separated by HPLC and quantified. **b**, *Ndst1*$^{f/f}$, *Ndst1*$^{-/-}$. **c**, WTa, *Ndst1*$^{f/f}$;*Ndst2*$^{-/-}$, *Ndst1*$^{-/-}$;*Ndst2*$^{-/-}$. **d**, *Ndst1*$^{f/f}$, *Glce*$^{-/-}$. **e**, *Hs2st1*$^{f/f}$, *Hs2st1*$^{-/-}$. **f**, *Hs6st1*$^{f/f}$, *Hs6st1*$^{-/-}$. **g**, WTa, *Hs6st1*$^{f/f}$;*Hs6st2*$^{-/-}$, *Hs6st1*$^{-/-}$;*Hs6st2*$^{-/-}$. **h**, *Sulf1*$^{f/f}$;*Sulf2*$^{f/f}$, *Sulf1*$^{-/-}$;*Sulf2*$^{-/-}$. **i**, *Ndst1*$^{f/f}$, *Hs3st1*$^{-/-}$, *Hs3st4*$^{-/-}$, *Hs3st1*$^{-/-}$;*Hs3st4*$^{-/-}$. We combined same-type sulfate groups, including NS, 2S, and 6S, of the separated disaccharides to assess the level of each type of sulfation modification. The data are summarized from 3 independent experiments and are presented as mean ± s.e.m. WTa ('wild-type' control) data were summarized from five similarly generated MLEC lines (*Ext1*$^{f/f}$, *Ndst1*$^{f/f}$, *Hs2st1*$^{f/f}$, *Hs6st1*$^{f/f}$, and *Sulf1*$^{f/f}$;*Sulf2*$^{f/f}$). We calculated the total number of sulfate groups by adding up NS, 2S, and 6S. **j**,**k**, Cell-surface antithrombin binding. Control (*Ndst1*$^{f/f}$) and *Hs3st*-mutant MLECs were stained with biotinylated antithrombin, and cell-surface-bound antithrombin was quantified by flow cytometry after further staining with fluorescein-tagged streptavidin. Representative histograms from 3 independent experiments are shown (**j**). The data for quantitation of mean fluorescence index are summarized from 3 independent experiments and are presented as mean ± s.d. (**k**). Statistical analyses were performed by two-sided Student's *t*-test.

showed slight reductions in 6S levels (NS 58.7%, 2S 17.3%, 6S 16.4% for *Ndst1*$^{f/f}$; NS 55.0%, 2S 20.1%, 6S 17.0% for *Hs3st1*$^{-/-}$; NS 55.7%, 2S 18.0%, 6S 10.7% for *Hs3st4*$^{-/-}$; NS 51.3%, 2S 18.9%, 6S 11.3% for *Hs3st1*$^{-/-}$;*Hs3st4*$^{-/-}$) (Fig. 2i, Table 1). We were not able to detect 3S in the disaccharide-composition assay and assessed it on the basis of binding of antithrombin, a ligand that strictly requires HS 3S for binding. *Hs3st1*$^{-/-}$ and *Hs3st4*$^{-/-}$ MLECs both showed reduced antithrombin binding compared with that in controls, and this effect was even more pronounced in *Hs3st1*$^{-/-}$;*Hs3st4*$^{-/-}$ cells (Fig. 2j,k), indicating that *Hs3st1* and *Hs3st4* deletion each reduce 3S. *Hs3st4*$^{-/-}$ and *Hs3st1*$^{-/-}$;*Hs3st4*$^{-/-}$ HS, but not *Hs3st1*$^{-/-}$ HS, showed slightly reduced overall sulfation compared with that in controls (*Hs3st4*$^{-/-}$, −10.6%; *Hs3st1*$^{-/-}$;*Hs3st4*$^{-/-}$, −12.3%) (Fig. 2i). *Hs6st1*$^{-/-}$, *Hs6st1*$^{f/f}$;*Hs6st2*$^{-/-}$, *Hs6st1*$^{-/-}$;*Hs6st2*$^{-/-}$, and *Sulf1*$^{-/-}$;*Sulf2*$^{-/-}$ HS had normal overall sulfation compared with that in the respective control lines. Thus, the combined examination of cells with mutations in *Hs6st*, *Sulf*, and *Hs3st* genes could allow researchers to determine and differentiate the importance of 3S, 6S, and overall sulfation for ligand binding and downstream signaling activation in these cells.

As a whole, the generated MLEC library harbors alterations of all HS modification types and might allow for determination of the necessity of specific modifications and overall HS sulfation levels for ligand binding and subsequent downstream signaling activation.

The importance of fine structure versus sulfation level of HS for FGF2–FGFR1 signaling. HS functions as a coreceptor for FGF signaling by interacting with FGF and FGFR to form functional FGF–HS–FGFR ternary complexes on the cell surface. FGF2 is one of the most studied HS-binding ligands, yet there is still debate about the relative importance of HS specific modifications and overall sulfation levels for FGF2 binding. Affinity binding and crystallography studies have demonstrated the necessity of NS and 2S for FGF2 binding, whereas 6S is required only to bridge FGF2 and FGFR for effective signaling activation, and not for FGF2 binding[13–16]. Biochemical studies also demonstrated that distinct HS structures differentially regulate FGF2 signaling via different FGFRs in a manner not related to sulfation level, which supports the idea that sulfation patterns are crucial[17]. However, some biochemical studies[6,7,18], in particular a genetic study of HS-mutant *Drosophila*[8], have suggested that the overall sulfation level is more important for FGF signaling than strictly defined HS fine structures are. Considering that HS deficiency in vivo can potentially affect multiple signaling pathways simultaneously, we reasoned that direct stimulation of HS-mutant MLECs, which expressed only FGFR1 at comparable levels among the cell lines used in this study (Supplementary Figs. 5–7), with FGF2 might allow this fundamental issue to be better addressed.

We assessed cell-surface FGF2 binding by flow cytometry after staining the cells with biotinylated FGF2. We assessed FGFR1 activation by measuring Erk1/2 phosphorylation. Deletion of *Ndst1*, *Ndst2*, or both *Ndst1* and *Ndst2* reduced NS levels and overall sulfation levels compared with those in controls. After FGF2 staining, the reductions in cell-surface FGF2 binding on *Ndst1*$^{-/-}$, *Ndst1*$^{f/f}$;*Ndst2*$^{-/-}$, and *Ndst1*$^{-/-}$;*Ndst2*$^{-/-}$ MLECs correlated with the levels of NS and overall sulfation in those cells, as well as with attenuated Erk1/2 phosphorylation (Fig. 3a, Table 2, Supplementary Figs. 8 and 9), which implies that certain levels of NS, overall sulfation, or both are required for HS to facilitate FGF2–FGFR1 signaling. Because *Ndst1* deletion also led to reduced 2S and 6S, examinations of *Hs2st1*$^{-/-}$ and *Hs6st1*$^{-/-}$;*Hs6st2*$^{-/-}$ cells are needed to better determine the importance of HS NS for FGF2–FGFR1 signaling.

Deletion of *Glce* and *Hs2st1* decreased epimerization and 2S, respectively, but slightly increased the overall sulfation of the mutant HS compared with that in controls. *Glce*$^{-/-}$ and *Hs2st1*$^{-/-}$ MLECs both showed significantly reduced FGF2 binding and attenuated downstream signaling compared with that in controls (Fig. 3b,c, Table 2, Supplementary Figs. 8 and 9), indicating that IdoA and 2S modifications are more important than the overall sulfation level for FGF2–FGFR1 signaling.

Deletion of *Hs6st1* reduced only 6S levels, and deletion of *Hs6st2* did not affect the HS disaccharide composition, whereas double deletion of *Hs6st1* and *Hs6st2* led to decreased 6S along with increased NS and 2S. Deletion of *Hs6st1*, *Hs6st2*, or both did not alter the overall sulfation level. The *Hs6st1*$^{-/-}$, *Hs6st1*$^{f/f}$;*Hs6st2*$^{-/-}$, and *Hs6st1*$^{-/-}$;*Hs6st2*$^{-/-}$ mutants showed increased cell-surface FGF2 binding compared with that in controls, and this change correlated with unchanged, increased, and attenuated Erk1/2 phosphorylation, respectively (Fig. 3d, Table 2, Supplementary Figs. 8 and 9). Double deletion of *Sulf1* and *Sulf2* increased 6S but did not alter the overall sulfation. The *Sulf1*$^{-/-}$;*Sulf2*$^{-/-}$ MLECs showed reduced FGF2 binding and slightly attenuated Erk1/2 phosphorylation compared with that in controls (Fig. 3e, Table 2, Supplementary Figs. 8 and 9). Therefore, the examination of cells with mutations in *Hs6st* and *Sulf* genes demonstrated that 6S is more important than the overall sulfation for FGF2 signaling and that proper 6S is required for HS to effectively facilitate FGF2 signaling. These observations also exemplify that cell-surface FGF2-binding capacity does not necessarily correlate positively with downstream signaling activation. Furthermore, *Hs6st2*$^{-/-}$ cells had a normal HS disaccharide composition but showed altered FGF2 binding and downstream signaling activation, which suggests that *Hs6st2* deletion alters the sulfated domains in HS.

Reduced cell-surface antithrombin binding indicated that deletion of *Hs3st1* or *Hs3st4* alone or of both *Hs3st1* and *Hs3st4* reduced 3S. Deletion of *Hs3st4*, but not of *Hs3st1*, and double deletion of *Hs3st1* and *Hs3st4* also substantially reduced 6S and slightly reduced the overall sulfation compared with that in controls. Cell-surface FGF2 binding was increased on *Hs3st4*$^{-/-}$ MLECs but remained unchanged on *Hs3st1*$^{-/-}$ and *Hs3st1*$^{-/-}$;*Hs3st4*$^{-/-}$ MLECs, and all the *Hs3st*-mutated MLECs showed normal Erk1/2 phosphorylation after FGF2 stimulation (Fig. 3f, Table 2, Supplementary Figs. 8 and 9). These results show that 3S is dispensable for HS facilitation of FGF2 signaling and demonstrate again that increased cell-surface FGF2 binding does not positively correlate with enhanced FGF2 signaling activation.

Our results demonstrate that NS, IdoA, and 2S are essential for HS binding to FGF2, but only in the presence of proper 6S modification can this binding effectively facilitate FGF2–FGFR1 signaling activation. Our data support the idea that HS fine structure is more important than overall sulfation for FGF2–FGFR1 signaling.

Characterization of anti-HS phage display antibody epitopes. Anti-HS phage display antibodies are commonly used to probe HS structure expression in tissue in situ[19]. However, their putative epitopes have been determined only on the basis of their binding capacity for chemically modified heparins and a limited number of synthetic HS oligosaccharides[20,21]. To address this, we examined our mutant library using the common anti-HS phage display antibodies AO4B08, EV3C3V, RB4EA12, and HS4C3 (Fig. 4a)[19–24]. We analyzed the mutant MLECs for antibody binding to cell-surface HS by flow cytometry. We observed positive staining for all four antibodies in *Ext1*$^{f/f}$ cells (Fig. 4b). Epitopes recognized by AO4B08 and EV3C3 are more abundant than the ones recognized by HS4C3 and RB4EA12. Compared with binding to *Ext1*$^{f/f}$ cells, antibody binding to *Ext1*$^{-/-}$ cells was largely lost for EV3C3, HS4C3, and RB4EA12, and was partially lost for AO4B08 (Fig. 4b), which shows that these antibodies indeed bind native HS.

Previous biochemical studies established that the AO4B08-binding epitope contains NS, 6S, IdoA, and an internal 2-O-sulfated IdoA residue[20,21,24] (Fig. 4a). In agreement with these reports, we observed that binding of AO4B08 was reduced on *Ndst1*$^{-/-}$,

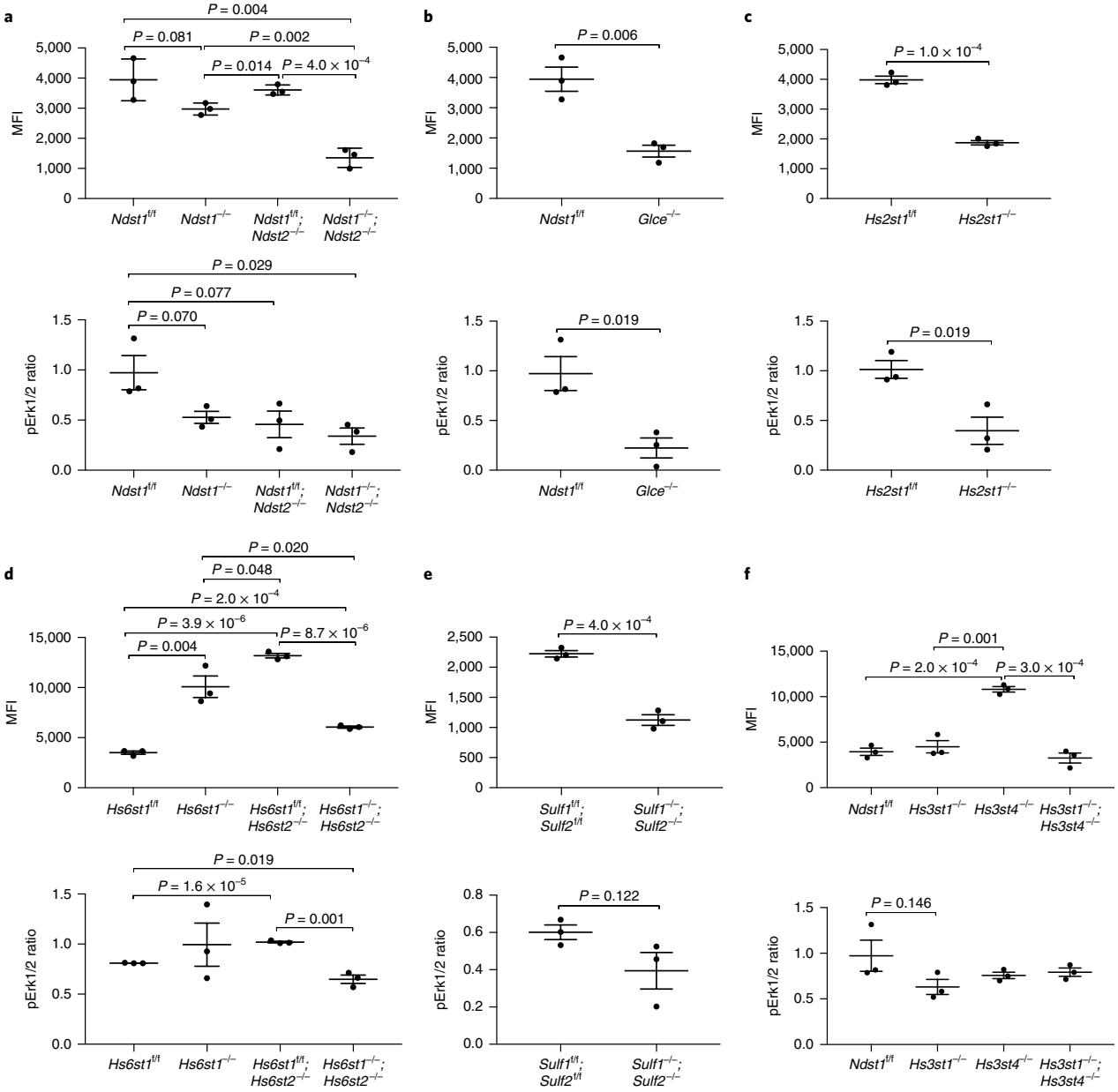

Fig. 3 | Effects of HS structure alteration on FGF2 binding and downstream Erk1/2 activation. The HS mutant MLECs and their controls were incubated with biotinylated FGF2, and the cell-surface-bound FGF2 was quantified by flow cytometry after staining with fluorescein-tagged streptavidin. In parallel, we stimulated the cells with FGF2, and assessed the resulting FGFR1 signaling activation by measuring pErk1/2 levels. **a**, *Ndst1*$^{f/f}$, *Ndst1*$^{-/-}$, *Ndst1*$^{f/f}$;*Ndst2*$^{-/-}$, *Ndst1*$^{-/-}$;*Ndst2*$^{-/-}$. **b**, *Ndst1*$^{f/f}$, *Glce*$^{-/-}$. **c**, *Hs2st1*$^{f/f}$, *Hs2st1*$^{-/-}$. **d**, *Hs6st1*$^{f/f}$, *Hs6st1*$^{-/-}$, *Hs6st1*$^{f/f}$;*Hs6st2*$^{-/-}$, *Hs6st1*$^{-/-}$;*Hs6st2*$^{-/-}$. **e**, *Sulf1*$^{f/f}$;*Sulf2*$^{f/f}$, *Sulf1*$^{-/-}$;*Sulf2*$^{-/-}$. **f**, *Ndst1*$^{f/f}$, *Hs3st1*$^{-/-}$, *Hs3st4*$^{-/-}$, *Hs3st1*$^{-/-}$;*Hs3st4*$^{-/-}$. The data are summarized from 3 independent experiments and are presented as mean ± s.d. Statistical analyses were performed by two-sided Student's *t*-test. MFI, mean fluorescence index.

Ndst1$^{f/f}$;*Ndst2*$^{-/-}$, *Ndst1*$^{-/-}$;*Ndst2*$^{-/-}$, *Glce*$^{-/-}$, *Hs2st1*$^{-/-}$, *Hs6st1*$^{-/-}$, *Hs6st1*$^{f/f}$;*Hs6st2*$^{-/-}$, and *Hs6st1*$^{-/-}$;*Hs6st2*$^{-/-}$ MLECs, whereas it was increased on *Sulf1*$^{-/-}$;*Sulf2*$^{-/-}$ MLECs (Fig. 4c–i). The binding of AO4B08 to *Hs3st1*$^{-/-}$, *Hs3st4*$^{-/-}$, and *Hs3st1*$^{-/-}$;*Hs3st4*$^{-/-}$ MLECs was also reduced (Fig. 4j), which indicates that the AO4B08 epitope contains 3S.

Biochemical studies have also shown that the EV3C3 epitope contains NS, IdoA, and 2S, and prefers a low level of 6S for good binding[20] (Fig. 4a). Compared with binding in controls, we observed reduced EV3C3 binding on *Ndst1*$^{-/-}$, *Ndst1*$^{f/f}$;*Ndst2*$^{-/-}$, *Ndst1*$^{-/-}$;*Ndst2*$^{-/-}$, *Glce*$^{-/-}$, *Hs2st1*$^{-/-}$, *Hs6st1*$^{-/-}$, *Hs6st1*$^{f/f}$;*Hs6st2*$^{-/-}$, and *Hs6st1*$^{-/-}$;*Hs6st2*$^{-/-}$ MLECs (Fig. 4c–h), which indicates that the EV3C3 epitope does contain NS, IdoA, 2S, and 6S. We noted increased EV3C3 binding to *Sulf1*$^{-/-}$;*Sulf2*$^{-/-}$ MLECs, which expressed HS with increased levels of 6S (Fig. 4i), thus indicating that higher 6S levels do not interfere with EV3C3 binding. These observations suggest that 6S is an essential component of the EV3C3 epitope. Binding of EV3C3 to *Hs3st1*$^{-/-}$, *Hs3st4*$^{-/-}$, and *Hs3st1*$^{-/-}$;*Hs3st4*$^{-/-}$ MLECs also was reduced (Fig. 4j), which indicates that the EV3C3 epitope contains 3S.

Table 2 | Effects of deletion of HS biosynthetic/remodeling genes on FGF2 binding and FGF2–FGFR1 signaling activation

Mutant	FGF2–FGFR1 signaling	
	FGF2 binding	Erk1/2 phosphorylation
Ndst1$^{-/-}$	~↓	~↓
Ndst1$^{f/f}$;*Ndst2*$^{-/-}$	~↓	~↓
Ndst1$^{-/-}$;*Ndst2*$^{-/-}$	↓	↓
Glce$^{-/-}$	↓	↓
Hs2st1$^{-/-}$	↓	↓
Hs6st1$^{-/-}$	↑	—
Hs6st1$^{f/f}$;*Hs6st2*$^{-/-}$	↑	↑
Hs6st1$^{-/-}$;*Hs6st2*$^{-/-}$	↑	↓
Hs3st1$^{-/-}$	—	—
Hs3st4$^{-/-}$	↑	—
Hs3st1$^{-/-}$;*Hs3st4*$^{-/-}$	—	—
Sulf1$^{-/-}$;*Sulf2*$^{-/-}$	↓	—

FGF2–FGFR1 signaling activation was assessed by measurement of downstream Erk1/2 phosphorylation. ↑, increased; ↓, attenuated; ~, slight alteration that did not reach statistical significance.

Biochemical studies have shown that the HS4C3 epitope contains NS, 2S, 6S, and 3S[19,22] (Fig. 4a). In agreement with these observations, we found that HS4C3 showed reduced binding on *Ndst1*$^{-/-}$, *Ndst1*$^{f/f}$;*Ndst2*$^{-/-}$, *Ndst1*$^{-/-}$;*Ndst2*$^{-/-}$, *Hs6st1*$^{-/-}$, *Hs6st1*$^{f/f}$;*Hs6st2*$^{-/-}$, *Hs6st1*$^{-/-}$;*Hs6st2*$^{-/-}$, *Hs3st1*$^{-/-}$, *Hs3st4*$^{-/-}$, and *Hs3st1*$^{-/-}$;*Hs3st4*$^{-/-}$ MLECs, but increased binding on *Sulf1*$^{-/-}$;*Sulf2*$^{-/-}$ MLECs (Fig. 4c,d,g–j). However, the binding of HS4C3 to *Hs2st1*$^{-/-}$ MLECs was unchanged compared with that in controls (Fig. 4f), indicating that the HS4C3 epitope does not necessarily have to contain the 2S modification. In addition, the binding of HS4C3 to *Glce*$^{-/-}$ MLECs was reduced compared with that in controls (Fig. 4e), which indicates that IdoA is an essential component of the HS4C3 epitope.

Previous biochemical studies determined that the RB4EA12 epitope contains N-acetylated and N-sulfated glucosamine residues with 6S modification[20] (Fig. 4a). This was supported in our study by reduced RB4EA12 binding on *Ndst1*$^{-/-}$, *Ndst1*$^{f/f}$;*Ndst2*$^{-/-}$, *Ndst1*$^{-/-}$;*Ndst2*$^{-/-}$, *Hs6st1*$^{-/-}$, *Hs6st1*$^{f/f}$;*Hs6st2*$^{-/-}$, and *Hs6st1*$^{-/-}$;*Hs6st2*$^{-/-}$ MLECs and increased binding on *Sulf1*$^{-/-}$;*Sulf2*$^{-/-}$ MLECs (Fig. 4c,d,g–i). *Hs2st1*$^{-/-}$ MLECs showed normal RB4EA12 binding compared with that in controls (Fig. 4f), indicating that the native HS epitope recognized by RB4EA12 does not necessarily have to contain 2S, in agreement with the reported biochemical analysis. RB4EA12 showed reduced binding to *Glce*$^{-/-}$, *Hs3st1*$^{-/-}$, *Hs3st4*$^{-/-}$, and *Hs3st1*$^{-/-}$;*Hs3st4*$^{-/-}$ MLECs (Fig. 4e–j), which suggests that the RB4EA12 epitope also contains IdoA and 3S.

Our HS-mutant cell-staining study determined the structural features of the native HS epitopes recognized by the four anti-HS phage antibodies, which, in most cases, were in good agreement with reported biochemical studies (Supplementary Table 1). However, we observed several discrepancies, including the requirement of 6S for EV3C3 and the lack of a requirement for 2S for HS4C3. In addition, we observed that 3S was a component of native HS epitopes for AO4B08, EV3C3, and RE4EA12. The 3S might have been additive, as the *Hs3st1*$^{-/-}$, *Hs3st4*$^{-/-}$, and *Hs3st1*$^{-/-}$;*Hs3st4*$^{-/-}$ MLECs showed only reduced antibody binding. Furthermore, the epitopes for HS4C3 and RB4EA12 also contained IdoA.

Characterization of the HS modification network in HS fine structure expression. HS biosynthesis is generally referred to as a sequential process consisting of initiation by copolymerases Ext1 and Ext2 followed by modification reactions initiated by Ndst-family enzymes and proceeded by Glce, Hs2st, Hs6st-family, and Hs3st-family enzymes. The biosynthesized HS is further subjected to extracellular remodeling by Sulf-family enzymes[5,9]. In HS composition analysis, we noticed that inactivation of an individual HS enzyme also affected upstream and/or downstream modifications that were not catalyzed by the mutant enzyme, which indicated that internal HS-modification network regulation exists in MLECs. We therefore correlated the disaccharide composition of the mutant HS with HS gene expression in the mutant cells to better understand the intermodification network regulation in MLECs.

Deletion of *Ndst1* led to upregulation of *Ndst3*, *Hs6st1*, and *Hs3st4* but downregulation of *Hs2st1* (Fig. 5a). *Ndst2* deletion did not affect the expression of other *Ndst* genes, but it led to upregulation of *Hs2st1*, *Hs3st4*, and *Sulf1* (Fig. 5b), thus showing that *Ndst1* and *Ndst2* have distinct regulation effects on other modification genes. *Ndst1* deletion reduced levels of NS and 6S but upregulated *Ndst3* and *Hs6st1*. Similarly, *Ndst2* deletion had no effect on 2S and 6S and upregulated *Hs2st1* and *Sulf1*. These observations indicate that, at the NS step, the modification network regulation occurs at the transcriptional level but contributes minimally to HS fine structure expression. Furthermore, simultaneous deletion of *Ndst1* and *Ndst2* diminished the network regulation, except for slight *Ndst3* upregulation (Fig. 5c, Supplementary Fig. 10a), indicating that the modification network regulation essentially depends on the expression of *Ndst* genes.

Glce deletion led to upregulation of *Ndst1*, *Ndst2*, *Hs2st1*, *Hs6st1*, and *Sulf2*, correlating with increased NS and 6S of HS (Fig. 5d), which indicates inhibitory regulation by *Glce* of NS and 6S via downregulation of *Ndst1*, *Ndst2*, and *Hs6st1*. Increased 6S in *Glce*$^{-/-}$ HS also indicated that the upregulation of *Sulf2* contributes minimally to 6S modification.

Hs2st1 deletion led to upregulation of *Ndst2*, *Glce*, *Hs6st1*, *Hs6st2*, *Hs3st1*, *Hs3st4*, *Hs3st6*, *Sulf1*, and *Sulf2* (Fig. 5e), thus revealing profound inhibition by *Hs2st1* of other modification genes. Similar to *Glce* deletion, *Hs2st1* deletion led to increased NS and 6S, indicating that *Hs2st1* inhibits NS and 6S by downregulating *Ndst2*, *Hs6st1*, and *Hs6st2*, and that the contributions of upregulated *Sulf1* and *Sulf2* remain minimal.

Hs6st1 deletion upregulated *Ndst1*, *Hs2st1*, *Hs3st1*, *Sulf1*, and *Sulf2* but did not affect NS and 2S (Fig. 5f). *Hs6st2* deletion upregulated *Hs6st1* and *Hs3st1* but did not alter 6S, NS, or 2S (Fig. 5g, Supplementary Fig. 10b). However, simultaneous deletion of *Hs6st1* and *Hs6st2* led to upregulation of *Ndst1*, *Ndst2*, *Hs2st1*, *Hs3st1*, and *Sulf2* (Fig. 5h), which correlated with increased NS and 2S, thus revealing inhibition of NS and 2S modification by *Hs6st* genes through suppression of *Ndst1*, *Ndst2*, and *Hs2st1* expression.

Hs3st1 deletion led to slight upregulation of *Ndst2* but downregulation of *Hs2st1* and *Hs3st4* (Fig. 5i), and did not alter HS composition. *Hs3st4* deletion led to slight upregulation of *Ndst1*, *Ndst2*, and *Hs3st1*; slight downregulation of *Hs2st1*; and high upregulation of *Sulf2* (Fig. 5j), which correlated with reduced 6S. Simultaneous deletion of *Hs3st1* and *Hs3st4* showed regulatory effects similar to those of *Hs3st4* deletion (Fig. 5k, Supplementary Fig. 10c–e), except for slight *Hs6st1* upregulation, indicating that, within the *Hs3st*-family genes expressed in MLECs, *Hs3st4* plays the major role in negative regulation of the modification network and has an overall role in increasing 6S.

Simultaneous deletion of *Sulf1* and *Sulf2* led to downregulation of *Ndst1*, *Ndst2*, and *Hs2st1*, and upregulation of *Glce* and *Hs3st1* (Fig. 5l), which correlated with reduced NS and 2S, indicating positive regulation by *Sulf* genes of NS and 2S and negative regulation of epimerization and 3S. Furthermore, the increased 6S levels in *Sulf1*$^{-/-}$;*Sulf2*$^{-/-}$ HS indicated that the overall 6S level is critically regulated by *Sulf* genes in MLECs.

In all, our systematic study reveals the following: (1) In MLECs, *Ndst* genes are essentially required in order for intermodification network regulation to occur, in good agreement with the modification-initiation function of *Ndst* genes in HS biosynthesis. (2) *Glce*,

a

Characteristics	Anti-HS phage display antibody			
	AO4B08	EV3C3	HS4C3	RB4EA12
Essential modifications	NS, C5-epimerization, 2S[a], 6S	NS, C5-epimerization, 2S	NS, 2S, 6S, 3S	NAc, NS, 6S
Inhibitory modifications		High 6S (possibly)		

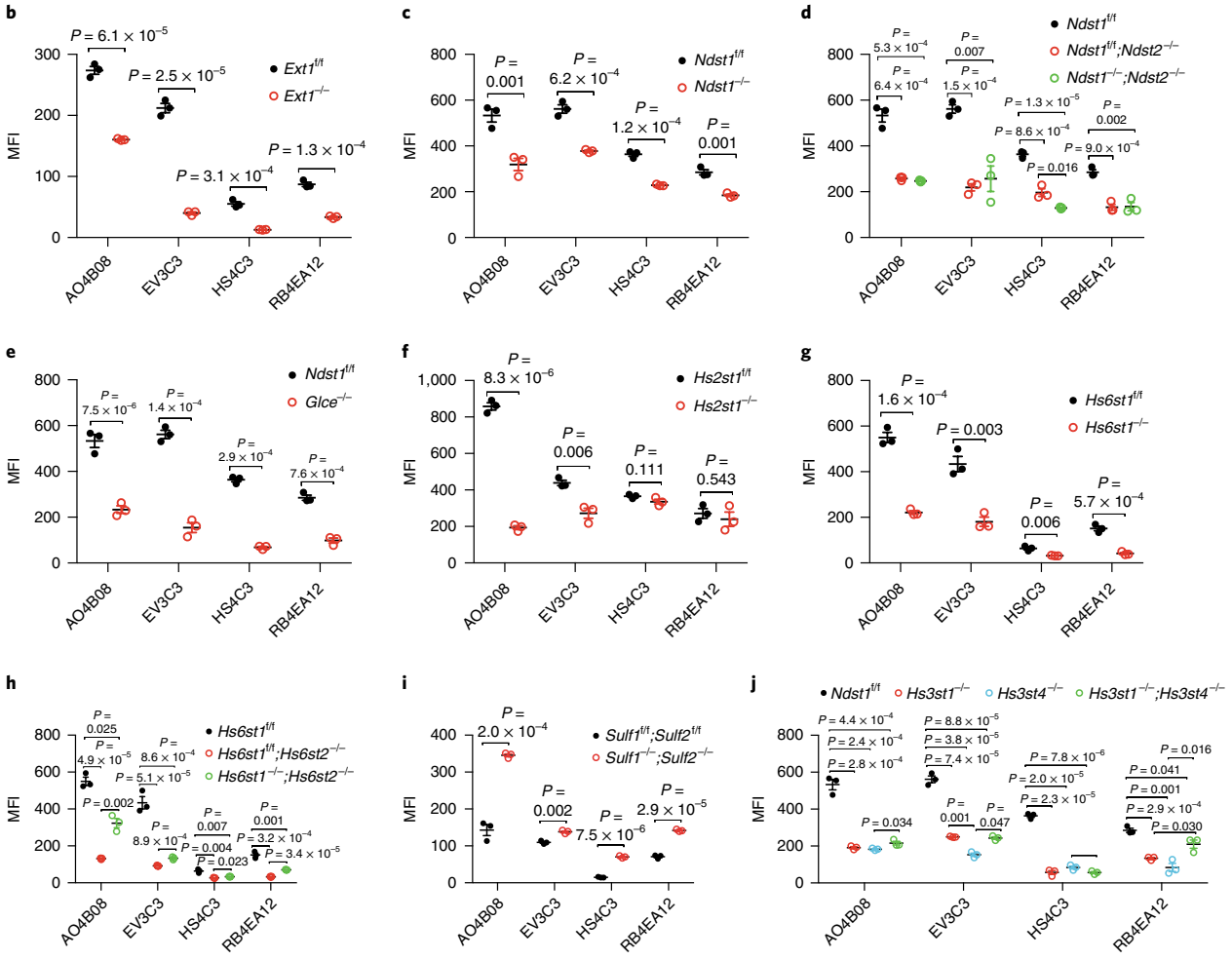

Fig. 4 | Binding of anti-HS phage display antibody to mutant HS on the endothelial cell surface. a, Summarized characteristics of the HS modifications involved in binding or binding inhibition of anti-HS phage display antibodies in reported biochemical studies. Antibody AO4B08 required an internal IdoA2S residue for binding. **b**–**j**, Cell-surface antibody binding. The HS mutant MLECs and their controls were incubated with VSV-G-tagged anti-HS phage display antibody, and the cell-surface-bound antibody was quantified by flow cytometry after staining with biotinylated anti-VSV-G antibody and fluorescein-tagged streptavidin. **b**, *Ext1*$^{f/f}$, *Ext1*$^{-/-}$. **c**, *Ndst1*$^{f/f}$, *Ndst1*$^{-/-}$. **d**, *Ndst1*$^{f/f}$, *Ndst1*$^{f/f}$;*Ndst2*$^{-/-}$, *Ndst1*$^{-/-}$;*Ndst2*$^{-/-}$. **e**, *Ndst1*$^{f/f}$, *Glce*$^{-/-}$. **f**, *Hs2st1*$^{f/f}$, *Hs2st1*$^{-/-}$. **g**, *Hs6st1*$^{f/f}$, *Hs6st1*$^{-/-}$. **h**, *Hs6st1*$^{f/f}$, *Hs6st1*$^{f/f}$;*Hs6st2*$^{-/-}$, *Hs6st1*$^{-/-}$;*Hs6st2*$^{-/-}$. **i**, *Sulf1*$^{f/f}$;*Sulf2*$^{f/f}$, *Sulf1*$^{-/-}$;*Sulf2*$^{-/-}$. **j**, *Ndst1*$^{f/f}$, *Hs3st1*$^{-/-}$, *Hs3st4*$^{-/-}$, *Hs3st1*$^{-/-}$;*Hs3st4*$^{-/-}$. The data are summarized from 3 independent experiments and are presented as mean ± s.d. Statistical analyses were performed by two-sided Student's *t*-test.

Hs2st1, *Hs6st* genes, and *Hs3st* genes reciprocally inhibit non-self-modification at the gene-expression and HS-composition levels. (3) *Sulf* genes positively regulate NS and 2S, but negatively regulate epimerization and 3S.

Regulation of HS chain length by HS gene expression. *Ndst2*, but not *Ndst1*, was reported to regulate HS chain length[25]. Currently we lack a systematic view of the HS chain-length regulation by HS genes. In PAGE analysis of intact HS, we determined that *Ndst1*$^{-/-}$ and *Hs3st1*$^{-/-}$;*Hs3st4*$^{-/-}$ HS had normal chain lengths compared with those in controls, whereas *Ndst2*$^{-/-}$, *Glce*$^{-/-}$, *Hs6st1*$^{f/f}$;*Hs6st2*$^{-/-}$, and *Hs3st1*$^{-/-}$ HS became shorter, and *Ndst1*$^{-/-}$;*Ndst2*$^{-/-}$, *Hs2st1*$^{-/-}$, *Hs6st1*$^{-/-}$, *Hs6st1*$^{-/-}$;*Hs6st2*$^{-/-}$, and *Hs3st4*$^{-/-}$ HS became longer (Supplementary Fig. 11). A comparison of single- and

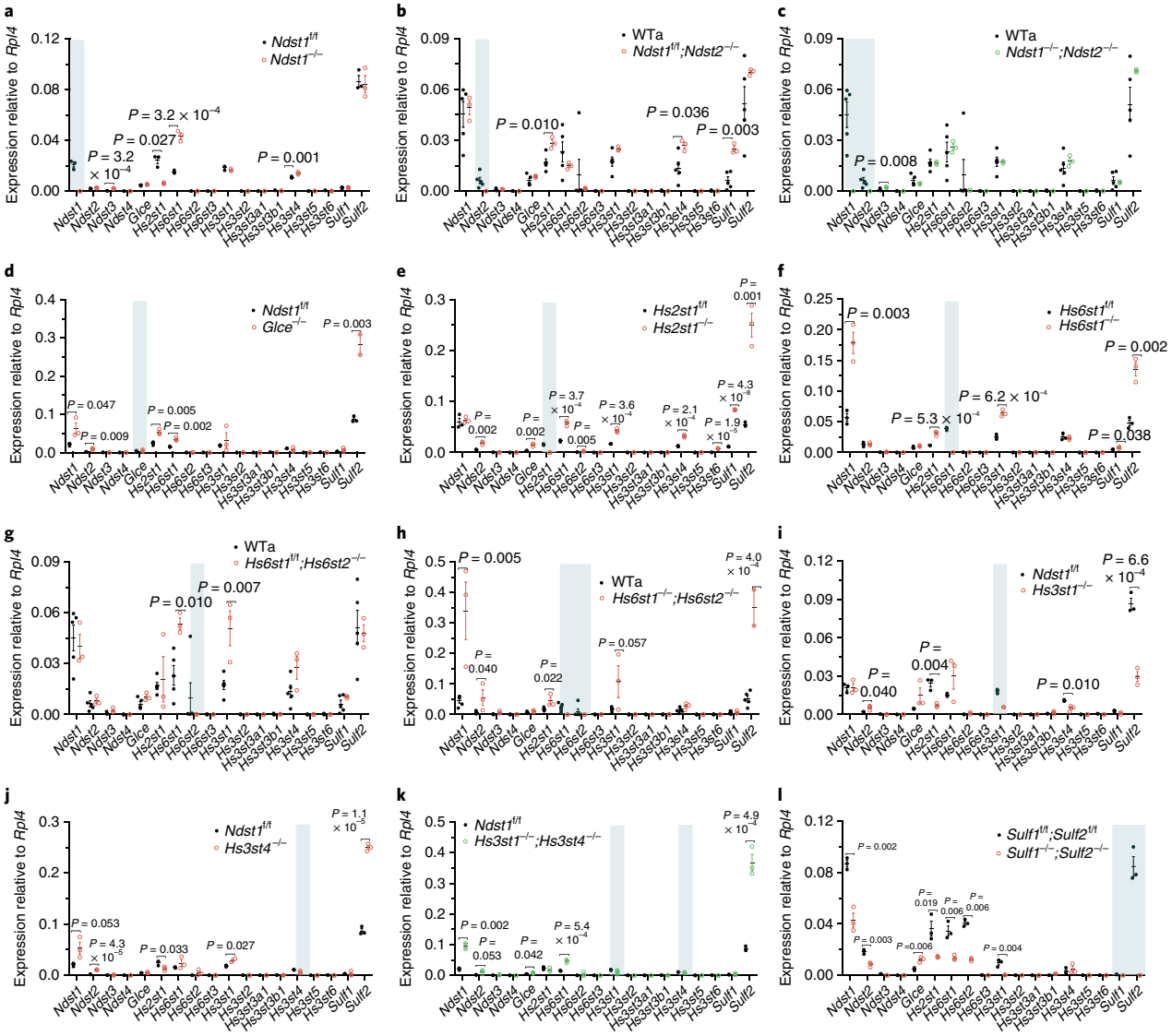

Fig. 5 | Inter-regulation among HS modification and remodeling genes in HS fine structure expression. The expression of HS modification and remodeling genes in the HS mutant MLECs and their controls as quantified by qRT-PCR analysis. The examined cell genotypes included *Ndst1*$^{f/f}$, *Ndst1*$^{-/-}$ (**a**); WTa, *Ndst1*$^{f/f}$;*Ndst2*$^{-/-}$ (**b**); WTa, *Ndst1*$^{-/-}$;*Ndst2*$^{-/-}$ (**c**); *Ndst1*$^{f/f}$, *Glce*$^{-/-}$ (**d**); *Hs2st1*$^{f/f}$, *Hs2st1*$^{-/-}$ (**e**); *Hs6st1*$^{f/f}$, *Hs6st1*$^{-/-}$ (**f**); WTa, *Hs6st1*$^{f/f}$;*Hs6st2*$^{-/-}$ (**g**); WTa, *Hs6st1*$^{-/-}$;*Hs6st2*$^{-/-}$ (**h**); *Ndst1*$^{f/f}$, *Hs3st1*$^{-/-}$ (**i**); *Ndst1*$^{f/f}$, *Hs3st4*$^{-/-}$ (**j**); *Ndst1*$^{f/f}$, *Hs3st1*$^{-/-}$;*Hs3st4*$^{-/-}$ (**k**); and *Sulf1*$^{f/f}$;*Sulf2*$^{f/f}$, *Sulf1*$^{-/-}$;*Sulf2*$^{-/-}$ (**l**). The data are summarized from 3 independent experiments and are presented as mean ± s.d. Statistical analyses were performed by two-sided Student's *t*-test. The targeted genes in the mutant MLECs are highlighted by shaded vertical bars.

double-gene-deficient HS showed that for genes in the same family, including *Ndst1* and *Ndst2*, *Hs6st1* and *Hs6st2*, and *Hs3st1* and *Hs3st4*, the two expressed genes had opposite regulation effects on HS chain length and reciprocally inhibited each other. All examined HS genes regulated HS chain length, and this regulation could be positive or negative, as well as direct or indirect.

Discussion

Examination of HS-mutant cells is an effective and straightforward approach for determining the function and structure–function relationships of native HS in a biological setting. This type of study was originally carried out with chemical-mutagenesis-generated HS-mutant CHO cell lines[26–28]. Currently only four CHO HS-mutant cell lines are available. CHO cells do not express *Hs3st* genes and cannot be used to examine 3S-related modifications[29,30]. CHO cells also lack endogenous expression of many HS-dependent signaling receptors, such as FGFR, receptors for vascular endothelial growth factor (VEGF), and Slit; very limited cellular function information has been obtained with these mutant CHO cells. Our examination of *Ndst1*$^{-/-}$ and *Ndst1*$^{f/f}$ MLEC lines determined that NS is required for HS to function as a coreceptor for VEGF and Slit3 signaling[31–34]. The success of previous studies and the FGF signaling coreceptor study described here demonstrate that our HS-mutant MLEC library represents a powerful platform for examining the roles and the structure–function relationship of HS in a cellular context, and findings could potentially be correlated with in vivo findings in corresponding mutant mice. In addition, our study demonstrates CRISPR–Cas9 technology as a highly efficient approach

to generate HS-mutant MLECs and is expected to be applicable to other cell types for the generation of HS mutants.

HS functions as a coreceptor for FGF signaling by interacting with both FGF and FGFR. A number of biochemical studies have shown that interactions of HS with FGFs require unique structures in which NS, 2S, and 6S contribute to the generation of specific sulfation patterns[15–17,35–37]. Crystallographic studies showed that 2S and 6S form hydrogen bonds with heparin-binding residues of FGFs and/or FGFRs to induce dimerization of FGFRs[14]. Meanwhile, other studies reported that FGF binding to HS is dictated primarily by the overall sulfation level, rather than by the precise positioning of various sulfate groups[7,8,18]. We observed that MLECs with knockout of *Glce*, *Hs2st1*, *Hs6st*-family genes, and *Sulf*-family genes, which express only FGFR1, showed altered FGF2 binding and downstream signaling activation, even though the mutants had normal or slightly increased HS overall sulfation. Our results support the idea that HS fine structure is more important than overall sulfation for FGF2–FGFR1 signaling activation.

HS phage display antibodies have been widely applied to probe HS structure in various tissues in situ[19,21,38]. However, their native HS epitope structures remain largely unclear[21,39]. Using our HS-mutant cell library, we found that (1) the EV3C3 epitope involves 6S, and a natural increase in 6S levels does not inhibit antibody binding; (2) the HS4C3 epitope does not necessarily contain 2S but requires IdoA; and (3) the epitopes for AO4B08, EV3C3, and RB4EA12 also require 3S. The involvement of rare 3S suggests that the antibodies may function in the 'all-or-nothing' high-specific-binding mode[40], thus supporting the application of the antibodies as high-affinity probes for specific HS structures in situ. Further studies with a comprehensive, synthesized, 3S-containing HS library might help further define the epitope structures.

Studies of *Hs2st1*-deficient CHO cells and mouse fibroblasts[41,42] and HS-deficient *Drosophila*[8] and *Caenorhabditis elegans*[43] revealed an inter-regulatory modification network in HS biosynthesis. Systematic perturbation of HS-modification genes in *C. elegans* led to the proposal of an inter-regulation model of modification enzymes in HS biosynthesis in metazoans: *Glce*, *Hs2st1*, and *Hs6st*-family genes inhibit NS; *Glce* stimulates both 2S and 6S; *Hs2st1* and the *Hs6st* genes inhibit 6S and 2S, respectively; and 6S is inhibited by *Sulf1*[43]. We observed similar inter-regulation in MLECs, except for *Glce*, which stimulated 2S but inhibited 6S, and *Sulf* genes, which also stimulated 2S. The discrepancy might be due to the fact that we examined only MLECs, whereas the *C. elegans* study examined the whole model organism. We also examined *Ndst* and *Hs3st* genes, and found that the inter-regulation network essentially depends on the expression of *Ndst* genes, and that *Hs3st4* stimulates 6S. In addition, we also observed that HS genes generally regulated HS chain length, by either elongating or shortening the chain, and HS genes within same family normally acted reciprocally to regulate HS chain length. These studies provide a comprehensive and systematic view of the inter-regulation of HS genes in mammalian cells at specific cell-type, transcription, and HS-structure levels. HS expression is cell-type specific, and similar studies with other cell types might determine whether our observed inter-regulation of HS expression is common in mammalian cells.

In the current study, HS structure analyses determined disaccharide composition and chain length, but not sequence, which plays the central role underpinning the structure–function relationship of HS. This should be examined once capable technology becomes available in the future.

Online content

Any methods, additional references, Nature Research reporting summaries, source data, statements of data availability and associated accession codes are available at https://doi.org/10.1038/s41592-018-0189-6.

Received: 2 February 2018; Accepted: 3 October 2018;
Published online: 30 October 2018

References

1. Bernfield, M. et al. Functions of cell surface heparan sulfate proteoglycans. *Annu. Rev. Biochem.* **68**, 729–777 (1999).
2. Esko, J. D. & Lindahl, U. Molecular diversity of heparan sulfate. *J. Clin. Invest.* **108**, 169–173 (2001).
3. Wang, L., Brown, J. R., Varki, A. & Esko, J. D. Heparin's anti-inflammatory effects require glucosamine 6-O-sulfation and are mediated by blockade of L- and P-selectins. *J. Clin. Invest.* **110**, 127–136 (2002).
4. Bishop, J. R., Schuksz, M. & Esko, J. D. Heparan sulphate proteoglycans fine-tune mammalian physiology. *Nature* **446**, 1030–1037 (2007).
5. Xu, D. & Esko, J. D. Demystifying heparan sulfate-protein interactions. *Annu. Rev. Biochem.* **83**, 129–157 (2014).
6. Jemth, P. et al. Biosynthetic oligosaccharide libraries for identification of protein-binding heparan sulfate motifs. Exploring the structural diversity by screening for fibroblast growth factor (FGF)1 and FGF2 binding. *J. Biol. Chem.* **277**, 30567–30573 (2002).
7. Kreuger, J. et al. Fibroblast growth factors share binding sites in heparan sulphate. *Biochem. J.* **389**, 145–150 (2005).
8. Kamimura, K. et al. Specific and flexible roles of heparan sulfate modifications in *Drosophila* FGF signaling. *J. Cell Biol.* **174**, 773–778 (2006).
9. Lindahl, U. & Li, J. P. Interactions between heparan sulfate and proteins—design and functional implications. *Int. Rev. Cell Mol. Biol.* **276**, 105–159 (2009).
10. Kraushaar, D. C., Yamaguchi, Y. & Wang, L. Heparan sulfate is required for embryonic stem cells to exit from self-renewal. *J. Biol. Chem.* **285**, 5907–5916 (2010).
11. Qiu, H. et al. Quantitative phosphoproteomics analysis reveals broad regulatory role of heparan sulfate on endothelial signaling. *Mol. Cell. Proteomics* **12**, 2160–2173 (2013).
12. Kraushaar, D. C. et al. Heparan sulfate facilitates FGF and BMP signaling to drive mesoderm differentiation of mouse embryonic stem cells. *J. Biol. Chem.* **287**, 22691–22700 (2012).
13. Faham, S., Hileman, R. E., Fromm, J. R., Linhardt, R. J. & Rees, D. C. Heparin structure and interactions with basic fibroblast growth factor. *Science* **271**, 1116–1120 (1996).
14. Schlessinger, J. et al. Crystal structure of a ternary FGF-FGFR-heparin complex reveals a dual role for heparin in FGFR binding and dimerization. *Mol. Cell* **6**, 743–750 (2000).
15. Turnbull, J. E., Fernig, D. G., Ke, Y., Wilkinson, M. C. & Gallagher, J. T. Identification of the basic fibroblast growth factor binding sequence in fibroblast heparan sulfate. *J. Biol. Chem.* **267**, 10337–10341 (1992).
16. Ashikari-Hada, S. et al. Characterization of growth factor-binding structures in heparin/heparan sulfate using an octasaccharide library. *J. Biol. Chem.* **279**, 12346–12354 (2004).
17. Guimond, S. E. & Turnbull, J. E. Fibroblast growth factor receptor signalling is dictated by specific heparan sulphate saccharides. *Curr. Biol.* **9**, 1343–1346 (1999).
18. Jastrebova, N. et al. Heparan sulfate-related oligosaccharides in ternary complex formation with fibroblast growth factors 1 and 2 and their receptors. *J. Biol. Chem.* **281**, 26884–26892 (2006).
19. van Kuppevelt, T. H., Dennissen, M. A., van Venrooij, W. J., Hoet, R. M. & Veerkamp, J. H. Generation and application of type-specific anti-heparan sulfate antibodies using phage display technology. Further evidence for heparan sulfate heterogeneity in the kidney. *J. Biol. Chem.* **273**, 12960–12966 (1998).
20. Dennissen, M. A. et al. Large, tissue-regulated domain diversity of heparan sulfates demonstrated by phage display antibodies. *J. Biol. Chem.* **277**, 10982–10986 (2002).
21. Thompson, S. M. et al. Heparan sulfate phage display antibodies identify distinct epitopes with complex binding characteristics: insights into protein binding specificities. *J. Biol. Chem.* **284**, 35621–35631 (2009).
22. Ten Dam, G. B. et al. 3-O-sulfated oligosaccharide structures are recognized by anti-heparan sulfate antibody HS4C3. *J. Biol. Chem.* **281**, 4654–4662 (2006).
23. Jenniskens, G. J., Oosterhof, A., Brandwijk, R., Veerkamp, J. H. & van Kuppevelt, T. H. Heparan sulfate heterogeneity in skeletal muscle basal lamina: demonstration by phage display-derived antibodies. *J. Neurosci.* **20**, 4099–4111 (2000).
24. Kurup, S. et al. Characterization of anti-heparan sulfate phage display antibodies AO4B08 and HS4E4. *J. Biol. Chem.* **282**, 21032–21042 (2007).
25. Deligny, A. et al. NDST2 (N-deacetylase/N-sulfotransferase-2) enzyme regulates heparan sulfate chain length. *J. Biol. Chem.* **291**, 18600–18607 (2016).

26. Bai, X., Wei, G., Sinha, A. & Esko, J. D. Chinese hamster ovary cell mutants defective in glycosaminoglycan assembly and glucuronosyltransferase I. *J. Biol. Chem.* **274**, 13017–13024 (1999).
27. Esko, J. D., Rostand, K. S. & Weinke, J. L. Tumor formation dependent on proteoglycan biosynthesis. *Science* **241**, 1092–1096 (1988).
28. Esko, J. D., Stewart, T. E. & Taylor, W. H. Animal cell mutants defective in glycosaminoglycan biosynthesis. *Proc. Natl. Acad. Sci. USA* **82**, 3197–3201 (1985).
29. Zhang, L., Lawrence, R., Frazier, B. A. & Esko, J. D. in *Methods in Enzymology* Vol. 416 (ed Fukuda, M.) 205–221 (Academic Press, New York, 2006).
30. Xu, X. et al. The genomic sequence of the Chinese hamster ovary (CHO)-K1 cell line. *Nat. Biotechnol.* **29**, 735–741 (2011).
31. Wijelath, E. et al. Multiple mechanisms for exogenous heparin modulation of vascular endothelial growth factor activity. *J. Cell. Biochem.* **111**, 461–468 (2010).
32. Zhang, B. et al. Heparan sulfate deficiency disrupts developmental angiogenesis and causes congenital diaphragmatic hernia. *J. Clin. Invest.* **124**, 209–221 (2014).
33. Qiu, H., Xiao, W., Yue, J. & Wang, L. Heparan sulfate modulates Slit3-induced endothelial cell migration. *Methods Mol. Biol.* **1229**, 549–555 (2015).
34. Zhang, B. et al. Repulsive axon guidance molecule Slit3 is a novel angiogenic factor. *Blood* **114**, 4300–4309 (2009).
35. Nakato, H. & Kimata, K. Heparan sulfate fine structure and specificity of proteoglycan functions. *Biochim. Biophys. Acta* **1573**, 312–318 (2002).
36. Habuchi, H., Habuchi, O. & Kimata, K. Sulfation pattern in glycosaminoglycan: does it have a code? *Glycoconj. J.* **21**, 47–52 (2004).
37. Maccarana, M., Casu, B. & Lindahl, U. Minimal sequence in heparin/heparan sulfate required for binding of basic fibroblast growth factor. *J. Biol. Chem.* **268**, 23898–23905 (1993).
38. Lensen, J. F. et al. Localization and functional characterization of glycosaminoglycan domains in the normal human kidney as revealed by phage display-derived single chain antibodies. *J. Am. Soc. Nephrol.* **16**, 1279–1288 (2005).
39. Powell, A. K., Yates, E. A., Fernig, D. G. & Turnbull, J. E. Interactions of heparin/heparan sulfate with proteins: appraisal of structural factors and experimental approaches. *Glycobiology* **14**, 17R–30R (2004).
40. Li, J. P. & Kusche-Gullberg, M. Heparan sulfate: biosynthesis, structure, and function. *Int. Rev. Cell Mol. Biol.* **325**, 215–273 (2016).
41. Bai, X. & Esko, J. D. An animal cell mutant defective in heparan sulfate hexuronic acid 2-O-sulfation. *J. Biol. Chem.* **271**, 17711–17717 (1996).
42. Merry, C. L. et al. The molecular phenotype of heparan sulfate in the *Hs2st*$^{-/-}$ mutant mouse. *J. Biol. Chem.* **276**, 35429–35434 (2001).
43. Townley, R. A. & Bülow, H. E. Genetic analysis of the heparan modification network in *Caenorhabditis elegans*. *J. Biol. Chem.* **286**, 16824–16831 (2011).

Acknowledgements

This research was supported by the NIH (R21HL131553, P41GM103390, 5R01HL093339, and U01CA225784 to L.W.; P01HL131474 and P01HL107150 to J.D.E.) and AHA (15POST21260001 and 17SDG33660550 to H.Q). S.S. and S.W. were supported by the Oversea Visiting Scholar Program for Middle-aged and Young Teachers in Shanghai Municipal Universities. We thank K. Howard for English-language revision of the manuscript. We also thank D. Bernsteel and H. Guo in the lab of M. Pierce at the University of Georgia (Athens, GA, USA) for providing the HT-29 cells, and J. Barber and J. Nelson in the flow cytometry core at the University of Georgia for their technical assistance.

Author contributions

H.Q. and L.W. conceived and designed the research and wrote the manuscript. H.Q. generated all the cell lines. H.Q., S.S., L.L., X.L., G.L., S.A.A.-H., S.W., P.A., F.Z., and R.J.L. designed and performed disaccharide analysis. R.J.L. also contributed to manuscript preparation. H.Q., M.X., and J.Y. performed western blotting. M.D.R., M.G., A.V.N., and K.W.M. performed the transcriptional analysis. T.H.v.K. provided the HS phage display antibodies and contributed to manuscript preparation. K.K., X.A., W.V.C., and J.D.E. provided the transgenic/knockout mice and contributed to manuscript preparation.

Competing interests

The authors declare no competing interests.

Additional information

Supplementary information is available for this paper at https://doi.org/10.1038/s41592-018-0189-6.

Reprints and permissions information is available at www.nature.com/reprints.

Correspondence and requests for materials should be addressed to L.W.

Publisher's note: Springer Nature remains neutral with regard to jurisdictional claims in published maps and institutional affiliations.

Methods

Cell derivation, immortalization, and gene knockout. *Ext1*$^{f/f}$[11,44], *Ndst1*$^{f/f}$[32,45], *Ndst1*$^{f/f}$;*Ndst2*$^{-/-}$[31,46], *Hs2st1*$^{f/f}$[47], *Hs6st1*$^{f/f}$[48], *Hs6st1*$^{f/f}$;*Hs6st2*$^{-/-}$[49], and *Sulf1*$^{f/f}$;*Sulf2*$^{f/f}$[50] mice on the C57BL/6 background were bred in accordance with regulations at the University of Georgia (UGA) and approved by the UGA Institutional Animal Care and Use Committee. Primary MLECs were isolated from adult mice and immortalized as previously described[11]. Briefly, lung was dissected from mice after perfusion, cut into small pieces, and digested with collagenase and dispase. The resultant cell suspension was subjected to phase separation with Histopaque 1088 (Sigma-Aldrich). The endothelial cells were enriched at the interface of PBS and Histopaque. The cells were further purified with anti-CD31-conjugated magnetic beads (Miltenyi Biotech). The isolated cells were cultured in gelatin-coated plates in high-glucose DMEM supplemented with 20% FBS (Atlanta Biologicals), 30 μg/ml endothelial cell growth supplement (Sigma-Aldrich), and 50 μg/ml heparin (Sigma-Aldrich). The primary cells were immortalized by transfection of a plasmid encoding SV40 large T antigen and subjected to single-cell cloning culture. After 7 d, single cell clones were picked out and expanded for future use. A plasmid encoding Cre recombinase was introduced into the cells by transient transfection to knock out the floxed genes in the obtained cell clones. The knockout cell lines were obtained by single-cell cloning culture, and targeted gene deletion was confirmed by genomic DNA genotyping as reported previously[45–49,51]. The genotype condition and primers are listed in Supplementary Table 2.

CRISPR–Cas9 procedure to generate knockout cell lines. We designed gRNAs for mouse *Glce*, *Hs3st1*, and *Hs3st4* by using the online CRISPR Design Tool (http://tools.genome-engineering.org) (Supplementary Fig. 4) and inserted them into the pCRISPR-LvSG03 plasmid (Genecopeia, USA). The gRNA and Cas9 plasmids were cotransfected into the *Ndst1*$^{f/f}$ MLEC line. The cells were selected by puromycin (10 μg/ml) for 3–7 d in culture and then were single-cell sorted into 96-well culture plates. The cell clones were screened for the targeted gene indel mutation by PCR amplification of the edited regions followed by enzyme mismatch assay after nuclease T7E1 digestion[52]. The selected clones were further validated by sequencing of the targeted regions. The sequence chromatograms of the pooled PCR products of the targeted regions were decoded by either DSDecodeM[53] or CRISP-ID[54] software online.

FGF2 biotinylation. A heparin–Sepharose CL-6B column was pre-equilibrated with binding buffer PB150 (17.9 mM Na_2HPO_4, 2.1 mM NaH_2PO_4, 150 mM NaCl, pH 7.8) and then loaded with FGF2 in the binding buffer. The flow-through was reloaded onto the column twice to ensure complete binding. After four washes with PB150, sulfo-NHS-biotin was added according to the manufacturer's instruction and incubated for 1 h at room temperature. The reaction was terminated by the addition of glycine (100 mM glycine in PB150). After washing of the column with gradient NaCl solutions (150 mM, 600 mM, and 1 M) in 20 mM PB buffer (44.75 mM Na_2HPO_4, 5.25 mM NaH_2PO_4, pH 7.8), biotinylated FGF2 was eluted with 4 M NaCl PB buffer, collected, and stored at −80 °C until use.

Flow cytometry analysis. MLECs were collected after digestion with PBS supplemented with 2 mM EDTA and 1% BSA (PBS-EB), and adjusted at 10^6 cells/ml. For FGF2 binding, the dissociated cells were incubated with biotinylated FGF2 (20 μg/ml) on ice for 30 min. Next, the cells were incubated with eFluor-450-conjugated streptavidin and then subjected to flow cytometry analysis (LSRII; BD Biosciences). For endothelial cell marker analysis, the cells were incubated with FITC-conjugated anti-mouse CD31 (eBioscience) or phycoerythrin-conjugated anti-mouse VEGFR2 antibody (BD Pharmingen) on ice for 30 min and then subjected to flow cytometry analysis. For HS phage display antibody staining, 10^6 MLECs in 100 μl of PBS-EB were incubated first with 10 μl of antibody (to AO4B08, HS4C3, RB4EA12, and EV3C3) on ice for 1 h and then with biotinylated anti-VSV-G (Abcam) on ice for 1 h after washing. After further incubation with streptavidin-conjugated eFluor 450 (eBioscience) and propidium iodide (25 μg/ml) for 30 min on ice, the cells were subjected to flow cytometry analysis. The flow cytometry data were processed and analyzed with FlowJo software.

Real-time polymerization chain reaction analysis. Cells in confluence were washed with PBS three times, flash-frozen in liquid nitrogen, and stored at −80 °C until use. Total RNA isolation, cDNA synthesis, qRT-PCR reactions, and data analysis were performed as previously reported[55]. The gene ribosomal protein L4 (*Rpl4*) was included as an internal control for normalization of individual gene expression.

HS disaccharide analysis. Cells were cultured in a 10-cm dish in high-glucose DMEM supplemented with 10% FBS and penicillin (100 U/ml) and streptomycin (100 μg/ml)[56,57]. After being washed with PBS-EB, the cells were lysed with 1 ml of 0.1 M NaOH. Next, we added 8 μl of acetic acid. The cell lysate was added with Pronase (2 mg/ml; Sigma-Aldrich) and digested overnight at 37 °C. After inactivation at 95 °C for 10 min, the released glycosaminoglycan was enriched by being passed through a Q-column, desalted, and then digested with heparin lyases I, II, and III (Sigma-Aldrich) overnight at 37 °C. We collected the resultant HS disaccharides by filtering the digested glycosaminoglycan though a 3,000 molecular-weight-cutoff (MWCO) filter (Thermo Fisher), labeling with 2-aminobenzide, and then carrying out separation with an Agilent 1260 HPLC system with a Propac PA1 (4 × 250 mm; DIONEX) column connected with a Propac PA1 Guard column (4 × 50 mm; DIONEX). The separated disaccharides were detected by a fluorescence detector with excitation at 348 nm and emission at 440 nm.

PAGE analysis of intact HS extracted from cell samples. Cell samples were first treated with 100 μl of protein-extraction reagent under sonication for 20 min[58,59]. To remove chondroitin sulfate and hyaluronic acid, we added recombinant chondroitin lyase and hyaluronidase (100 mU each) and 500 μl of digestion buffer (50 mM ammonium acetate, 2 mM calcium chloride) to the reaction buffer and incubated the samples under 37 °C for 2 h. Next, 0.1 ml of actinase E solution (20 mg/ml) was mixed with each sample for proteolysis at 55 °C for 24 h. HS was then recovered and purified with a Vivapure MINI Q spin column. We desalted the obtained product solution by passing it through 3 kDa MWCO spin columns, lyophilizing it, and finally redispersing it in 10 μl of deionized water for further use.

An analytical PAGE gel with 5 ml of 15% total acrylamide monomer resolving solution was allowed to polymerize for 30 min with 5 μl of TEMED and 30 μl of 10% (w/v) ammonium persulfate. Above the polymerized resolving gel, 2 ml of 5% total acrylamide monomer stacking gel was cast. An aliquot of 5 μl of purified HS was loaded in a solution of 10 μg/ml (w/v) phenol red and 25% (w/v) sucrose. Electrophoresis was conducted for 30 min at a constant voltage of 200 V.

Western blotting. Cells (2×10^5 cells/well) were seeded in six-well plates and cultured overnight in high DMEM supplemented with 10% FBS. Prior to stimulation, the cells were starved in DMEM serum-free culture conditions for 1 h. The cells were incubated with DMEM supplemented with FGF2 (5 ng/ml) for 15 min and then lysed with RIPA buffer containing protease and phosphatase inhibitors (Sigma-Aldrich). The resultant cell lysate was resolved on 7.5% SDS–PAGE, transferred onto nitrocellulose membrane, and blotted with anti-phospho-Erk1/2 (Cell Signaling Technology) and anti-Erk1/2 (Cell Signaling Technology) antibodies at 1:1,000. The HS-dependent FGF2-induced intracellular signaling activation was calculated as follows: Erk1/2 activation ratio = $((\text{p-Erk}_{1/2}/\text{T-Erk1/2})_{\text{FGF2}} - (\text{p-Erk}_{1/2}/\text{T-Erk1/2})_{\text{control}})^{\text{mutant}}/((\text{p-Erk}_{1/2}/\text{T- Erk}_{1/2})_{\text{FGF2}} - (\text{p-Erk}_{1/2}/\text{T-Erk}_{1/2})_{\text{control}})^{\text{wildtype}}$. For FGFR expression analysis, the untreated cell lysate was subjected to 8% SDS–PAGE separation, transferred to nitrocellulose membrane, and blotted with anti-FGFR1 (D8E4; Cell Signaling Technology) or anti-FGFR2 (D4L2V; Cell Signaling Technology) antibodies at 1:1,000 dilution to determine the protein expression levels of FGFR1 and FGFR2 in the cell lines. We also determined the β-actin in the cell lysate for use as an internal control by blotting the membrane with monoclonal anti-β-actin (A2228). The results were imaged with KwikQuant imager (Kindle Bioscience, USA). The quantitation was based on the densitometry of the western blot bands.

Statistical analysis. For statistical analysis we used two-sided Student's *t*-test, with $P < 0.05$ considered statistically significant.

Resource availability. All cell lines are available on request under a standard material transfer agreement with UGA for academic research purposes.

Reporting Summary. Further information on research design is available in the Nature Research Reporting Summary linked to this article.

Data availability

All data generated or analyzed during this study are included in this article and/or its associated Supplementary Information files. The raw data files are available from the corresponding author upon request. Source data for Figs. 1–5 and Supplementary Figs. 3, 5, and 10 are available online.

References

44. Inatani, M., Irie, F., Plump, A. S., Tessier-Lavigne, M. & Yamaguchi, Y. Mammalian brain morphogenesis and midline axon guidance require heparan sulfate. *Science* **302**, 1044–1046 (2003).
45. Wang, L., Fuster, M., Sriramarao, P. & Esko, J. D. Endothelial heparan sulfate deficiency impairs L-selectin- and chemokine-mediated neutrophil trafficking during inflammatory responses. *Nat. Immunol.* **6**, 902–910 (2005).
46. Forsberg, E. et al. Abnormal mast cells in mice deficient in a heparin-synthesizing enzyme. *Nature* **400**, 773–776 (1999).
47. Stanford, K. I. et al. Heparan sulfate 2-O-sulfotransferase is required for triglyceride-rich lipoprotein clearance. *J. Biol. Chem.* **285**, 286–294 (2010).
48. Izvolsky, K. I., Lu, J., Martin, G., Albrecht, K. H. & Cardoso, W. V. Systemic inactivation of Hs6st1 in mice is associated with late postnatal mortality without major defects in organogenesis. *Genesis* **46**, 8–18 (2008).
49. Sugaya, N., Habuchi, H., Nagai, N., Ashikari-Hada, S. & Kimata, K. 6-O-sulfation of heparan sulfate differentially regulates various fibroblast growth factor-dependent signalings in culture. *J. Biol. Chem.* **283**, 10366–10376 (2008).

50. Tran, T. H., Shi, X., Zaia, J. & Ai, X. Heparan sulfate 6-O-endosulfatases (Sulfs) coordinate the Wnt signaling pathways to regulate myoblast fusion during skeletal muscle regeneration. *J. Biol. Chem.* **287**, 32651–32664 (2012).
51. Nagai, N. et al. Involvement of heparan sulfate 6-O-sulfation in the regulation of energy metabolism and the alteration of thyroid hormone levels in male mice. *Glycobiology* **23**, 980–992 (2013).
52. Vouillot, L., Thélie, A. & Pollet, N. Comparison of T7E1 and surveyor mismatch cleavage assays to detect mutations triggered by engineered nucleases. *G3 (Bethesda)* **5**, 407–415 (2015).
53. Liu, W. et al. DSDecode: a web-based tool for decoding of sequencing chromatograms for genotyping of targeted mutations. *Mol. Plant* **8**, 1431–1433 (2015).
54. Dehairs, J., Talebi, A., Cherifi, Y. & Swinnen, J. V. CRISP-ID: decoding CRISPR mediated indels by Sanger sequencing. *Sci. Rep.* **6**, 28973 (2016).
55. Nairn, A. V. et al. Glycomics of proteoglycan biosynthesis in murine embryonic stem cell differentiation. *J. Proteome Res.* **6**, 4374–4387 (2007).
56. Volpi, N. & Linhardt, R. J. High-performance liquid chromatography-mass spectrometry for mapping and sequencing glycosaminoglycan-derived oligosaccharides. *Nat. Protoc.* **5**, 993–1004 (2010).
57. Skidmore, M. A., Guimond, S. E., Dumax-Vorzet, A. F., Yates, E. A. & Turnbull, J. E. Disaccharide compositional analysis of heparan sulfate and heparin polysaccharides using UV or high-sensitivity fluorescence (BODIPY) detection. *Nat. Protoc.* **5**, 1983–1992 (2010).
58. Park, Y., Yu, G., Gunay, N. S. & Linhardt, R. J. Purification and characterization of heparan sulphate proteoglycan from bovine brain. *Biochem. J.* **344**, 723–730 (1999).
59. Chen, Y., Reddy, M., Yu, Y., Zhang, F. & Linhardt, R. J. Glycosaminoglycans from chicken muscular stomach or gizzard. *Glycoconj. J.* **34**, 119–126 (2017).

nature research

Corresponding author(s): Lianchun Wang

Life Sciences Reporting Summary

Nature Research wishes to improve the reproducibility of the work that we publish. This form is intended for publication with all accepted life science papers and provides structure for consistency and transparency in reporting. Every life science submission will use this form; some list items might not apply to an individual manuscript, but all fields must be completed for clarity.

For further information on the points included in this form, see Reporting Life Sciences Research. For further information on Nature Research policies, including our data availability policy, see Authors & Referees and the Editorial Policy Checklist.

Please do not complete any field with "not applicable" or n/a. Refer to the help text for what text to use if an item is not relevant to your study.
For final submission: please carefully check your responses for accuracy; you will not be able to make changes later.

Experimental design

1. Sample size

   Describe how sample size was determined.

   No sample size calculation was performed since the this is cell line study.

2. Data exclusions

   Describe any data exclusions.

   One transcript data of a triple repeat was excluded due to obvious abnormal value (less than mean of the triple- 3xSD)

3. Replication

   Describe the measures taken to verify the reproducibility of the experimental findings.

   The reproducibility of our experimental finding were confirmed by at least three independent repeat experiments.

4. Randomization

   Describe how samples/organisms/participants were allocated into experimental groups.

   No randomization was performed as the study are based on cells in different genotype.

5. Blinding

   Describe whether the investigators were blinded to group allocation during data collection and/or analysis.

   The heparan sulfate disaccharide, gene transcript and FGF2 signaling analyses were blind to the investigators. However, the cell surface staining for CD31, VEGFR2, anti-heparan sulfate phage display antibodies and genotyping were not blind to the investigators, because these information were needed essentially to generate the heparan sulfate mutant cell library.

Note: all in vivo studies must report how sample size was determined and whether blinding and randomization were used.

6. Statistical parameters

   For all figures and tables that use statistical methods, confirm that the following items are present in relevant figure legends (or in the Methods section if additional space is needed).

n/a	Confirmed
☐	☒ The exact sample size (*n*) for each experimental group/condition, given as a discrete number and unit of measurement (animals, litters, cultures, etc.)
☐	☒ A description of how samples were collected, noting whether measurements were taken from distinct samples or whether the same sample was measured repeatedly
☐	☒ A statement indicating how many times each experiment was replicated
☐	☒ The statistical test(s) used and whether they are one- or two-sided *Only common tests should be described solely by name; describe more complex techniques in the Methods section.*
☒	☐ A description of any assumptions or corrections, such as an adjustment for multiple comparisons
☐	☒ Test values indicating whether an effect is present *Provide confidence intervals or give results of significance tests (e.g. P values) as exact values whenever appropriate and with effect sizes noted.*
☐	☒ A clear description of statistics including central tendency (e.g. median, mean) and variation (e.g. standard deviation, interquartile range)
☐	☒ Clearly defined error bars in all relevant figure captions (with explicit mention of central tendency and variation)

See the web collection on statistics for biologists for further resources and guidance.

Software

Policy information about availability of computer code

7. Software

Describe the software used to analyze the data in this study.	Microsoft Excel 2017, Flowjo v8.7 for mac, DSDecodedM (http://skl.scau.edu.cn/dsdecode/), CRISP-ID (http://crispid.gbiomed.kuleuven.be/), CRISPR gRNA design tool (http://tools.genome-engineering.org)

For manuscripts utilizing custom algorithms or software that are central to the paper but not yet described in the published literature, software must be made available to editors and reviewers upon request. We strongly encourage code deposition in a community repository (e.g. GitHub). *Nature Methods* guidance for providing algorithms and software for publication provides further information on this topic.

Materials and reagents

Policy information about availability of materials

8. Materials availability

Indicate whether there are restrictions on availability of unique materials or if these materials are only available for distribution by a third party.	The unique heparan sulfate mouse lung endothelial cell lines were generated in our own laboratory and have been available to researchers in scientific field. To dates, we have shared the cell library with several laboratories world wide.

9. Antibodies

Describe the antibodies used and how they were validated for use in the system under study (i.e. assay and species).	The commercial antibodies were widely used and validated in many publications. The anti-heparan sulfate phage display antibodies have been used widely in the heparan sulfate field and validated in many publications too. In our study, we also validated the antibodies are true anti-heapran sulfate antibody using our heparan sulfate-deficient cells. PE-rat anti-mouse VEGFR2 antibody, BD Pharmingen (555308) PE-rat anti-mouse IgG2ak isotype control, BD Pharmingen (553930) CD31 Microbeads, mouse Miltenyibiotec (130-097-418) FITC rat IgG2ak isotype control, eBioscience (11-4321-80) FITC-anti-mouse CD31 antibody, eBioscience (11-0311-82) Anti-heparan aulfate antibody (10E4), amsbio (F58-10E4 clone) Biotin-anti-mouse IgM Monoclonal antibody, eBioscience (13-5790-82) eFluor 450-Streptavidin, eBioscience (48-4317-82) Anti-heparan Sulfate Display Antibodies including EV3C3, AO4B08, HS4C3, RB4EA12 were generated in Dr. Toin H. van Kuppevelt laboratory Biotinylated-anti-VSV-G antibody, Abcam, (Ab34774) Anti-Phospho-p42/p44 MAPK(Erk1/2)(Thr202/Tyr204) antibody ,Cell Signaling Technology (#9101) Anti-p42/p44 MAPK(Erk1/2)(Thr202/Tyr204) antibody, Cell Signaling Technology(#4695) Anti-FGFR1 antibody (clone D8E4) Cell Signaling Technology (#9740) Anti-FGFR2 antibody (clone D4L2V), Cell Signaling Technology (#23328) Anti-beta-actin antibody (clone AC-74), Sigma-Aldrich (# A2228)

10. Eukaryotic cell lines

a. State the source of each eukaryotic cell line used.	All the used mouse lung endothelial cell lines were generated in our own laboratory.
b. Describe the method of cell line authentication used.	The mouse lung endothelial cell lines were authenticated by observing cell surface expression of CD31 and VEGFR2 in flowcytomertry (flow cytometry BD LSRII).
c. Report whether the cell lines were tested for mycoplasma contamination.	All our cell lines have not tested for mycoplasma contamination.
d. If any of the cell lines used are listed in the database of commonly misidentified cell lines maintained by ICLAC, provide a scientific rationale for their use.	No commonly misidentified cell lines were used.

Animals and human research participants

Policy information about studies involving animals; when reporting animal research, follow the ARRIVE guidelines

11. Description of research animals

Provide all relevant details on animals and/or animal-derived materials used in the study.	All mice in C57BL6 background at 8-10 weeks-old were used including genetically engineered Ext1f/f, Ndst1f/f, Ndst2-/-, Hs2stf/f, Hs6st1f/f, Hs6st2-/-, Sulf1f/f;2f/f mice.

Policy information about studies involving human research participants

12. Description of human research participants

Describe the covariate-relevant population characteristics of the human research participants.	The study did not involve human research participants.